Supplementary Information

New Core-expanded Calix[4]pyrroles and N-donor-extended Dipyrromethanes: Syntheses, Anion Binding and Conformational Studies

Soumya Mishra,[a],§ Monalisa Giri,[a],§ Vipin Kumar Mishra,[b] and Tapas Guchhait*[a]

[a] Department of Chemistry, C. V. Raman Global University, Odisha, Bhubaneswar-752054, India.

E-mail: tguchhait@cgu-odisha.ac.in or guchhaittapas07@gmail.com

[b] Chemistry Division, School of Advanced Sciences and Languages, VIT Bhopal University, Bhopal, Madhya Pradesh-466114, India.

E-mail: vipinpandit13@gmail.com

* Corresponding author, § These authors have equal contribution to this work

Experimental Section

General

All reactions were carried out using standard Schlenk-line techniques under a nitrogen atmosphere. Solvents were distilled under N_2 atmosphere according to the standard procedures. Other chemicals were obtained from commercial sources and used as received. Dipyrromethanes were prepared as reported.[1] ^{1}H NMR (400 MHz and 700 MHz) and ^{13}C NMR (100 MHz and 175 MHz) spectra were recorded on Bruker Avance Neo 400 NMR and Bruker Avance III HD 700 NMR spectrometers. Chemical shifts were referenced with respect to the chemical shifts of the residual protons present in deuterated solvents. ATR spectra were recorded using a PerkinElmer Spectrum Rx. instrument. High-resolution mass spectra (ESI) were recorded using a XEVO G2XSQTOF (Waters) and Agilent AdvanceBio 6545XT LC/Q-TOF mass spectrometer. Melting points were determined in open capillaries and are corrected using benzophenone as a reference. UV-vis titration experiments were carried out using a Systronics (model 119) spectrophotometer. Binding constants (K_a) were calculated using the BindFit v0.5 software. X-ray structures were drawn using Mercury 4.2.0 software.[2] Room temperature is 25 °C. DFT studies were conducted using Gaussian software at the B3LYP/6-31G level.[3]

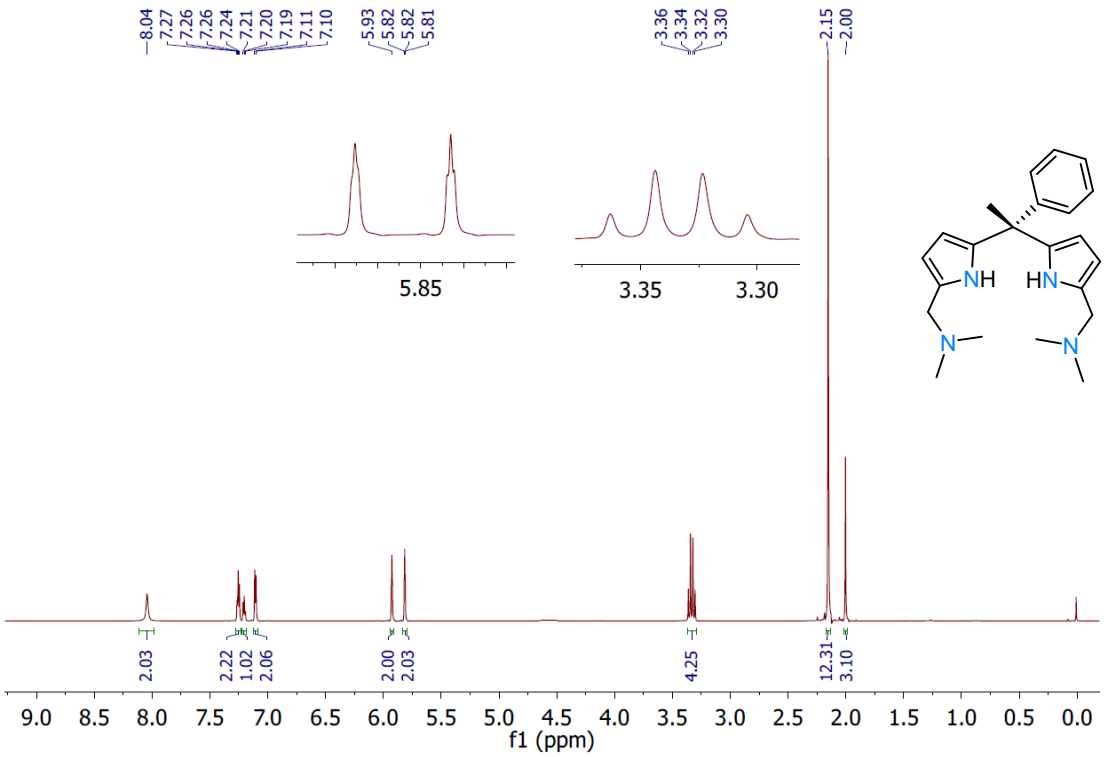

Figure S1: ^{1}H NMR (700 MHz) spectrum of **2b** in $CDCl_3$ at room temperature.

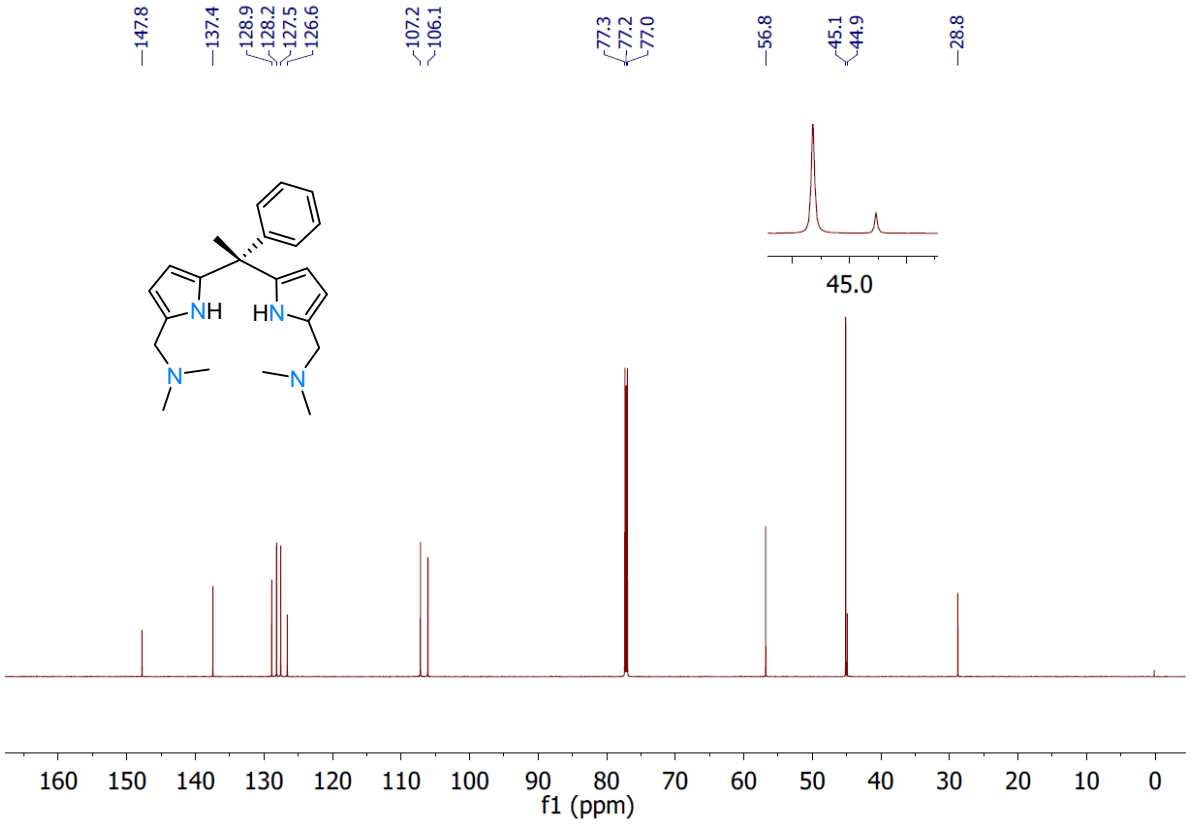

Figure S2: $^{13}C\{^{1}H\}$ NMR (175 MHz) spectrum of **2b** in $CDCl_3$ at room temperature.

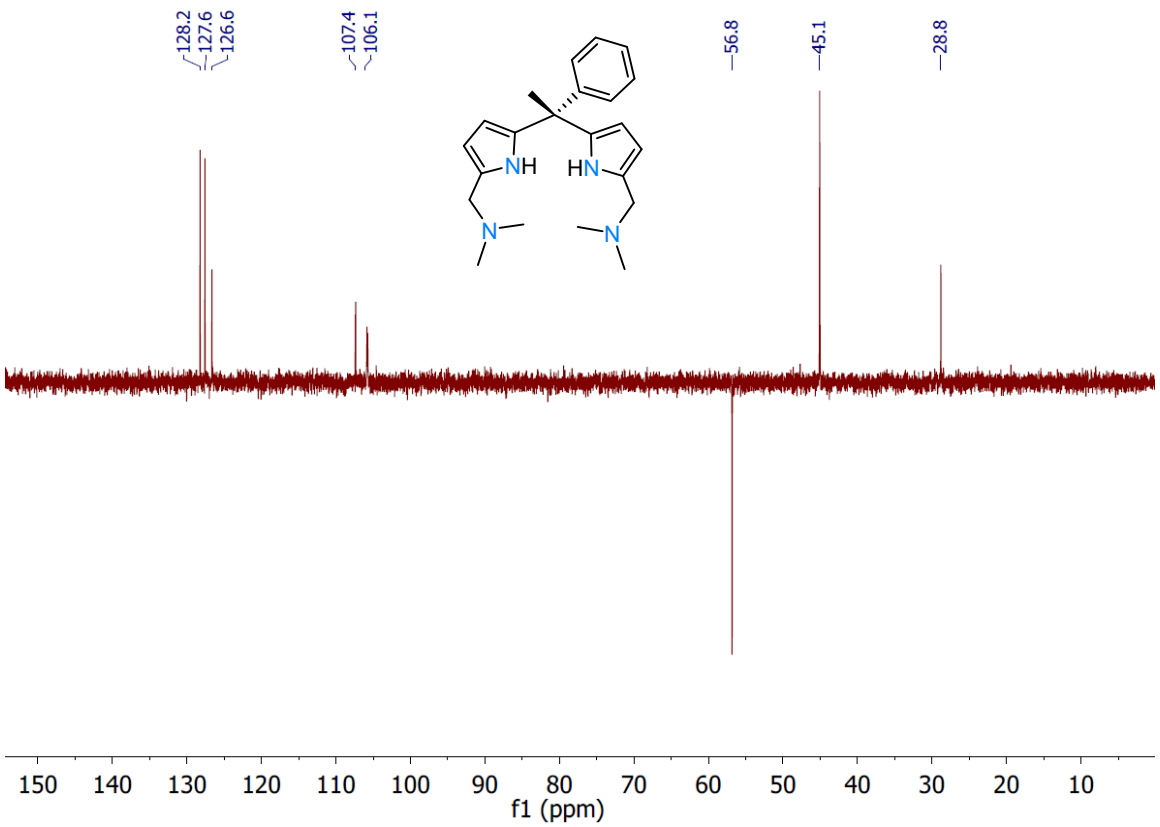

Figure S3: DEPT-135{^{1}H} NMR (175 MHz) spectrum of **2b** in $CDCl_3$ at room temperature.

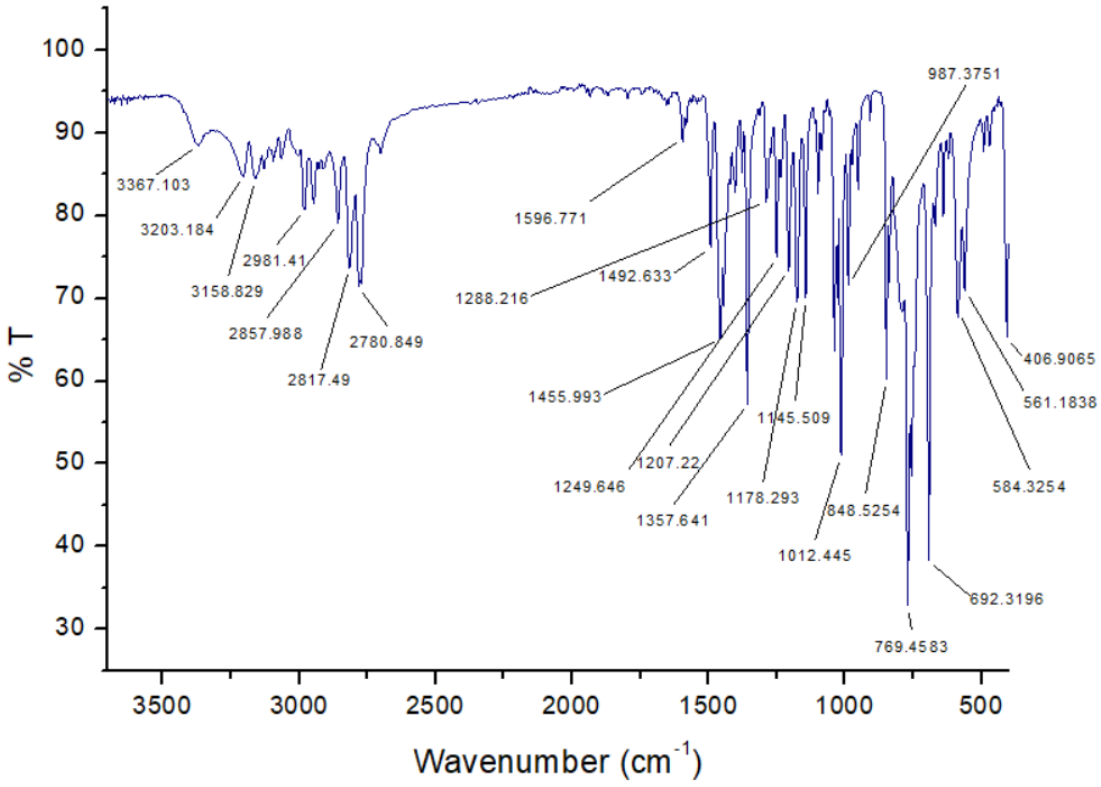

Figure S4: ATR spectrum of **2b**.

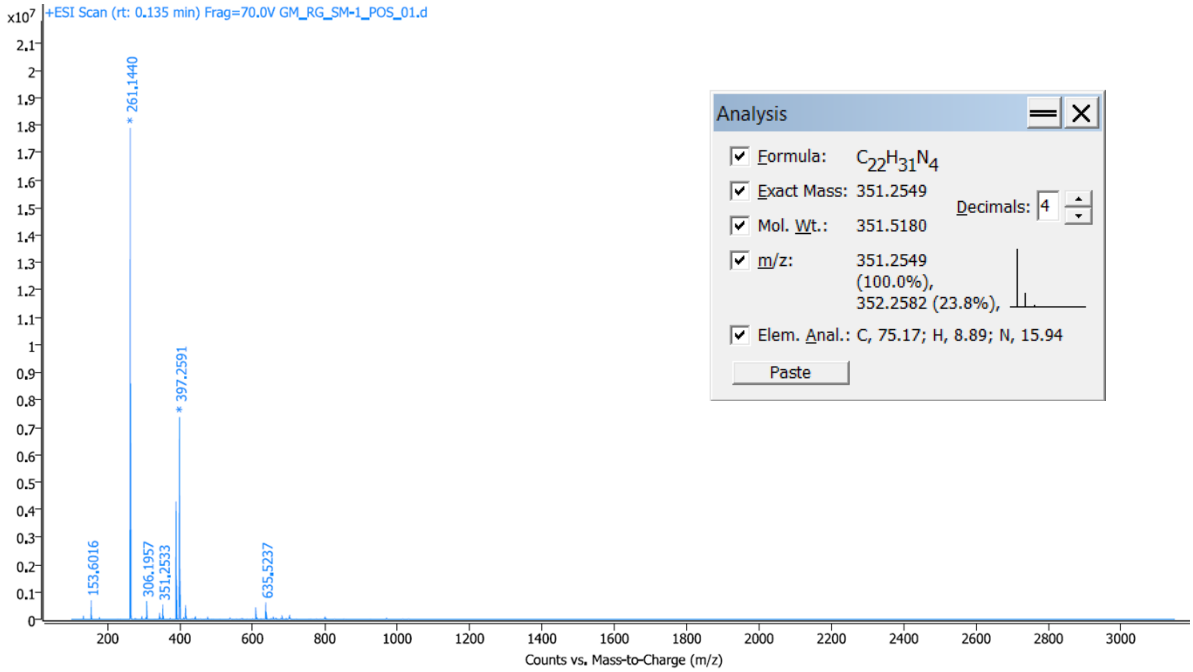

Figure S5: HRMS (ESI+) spectrum of **2b**, showing $[M+H]^+$ peak at 351.2533 (calcd: 351.2549).

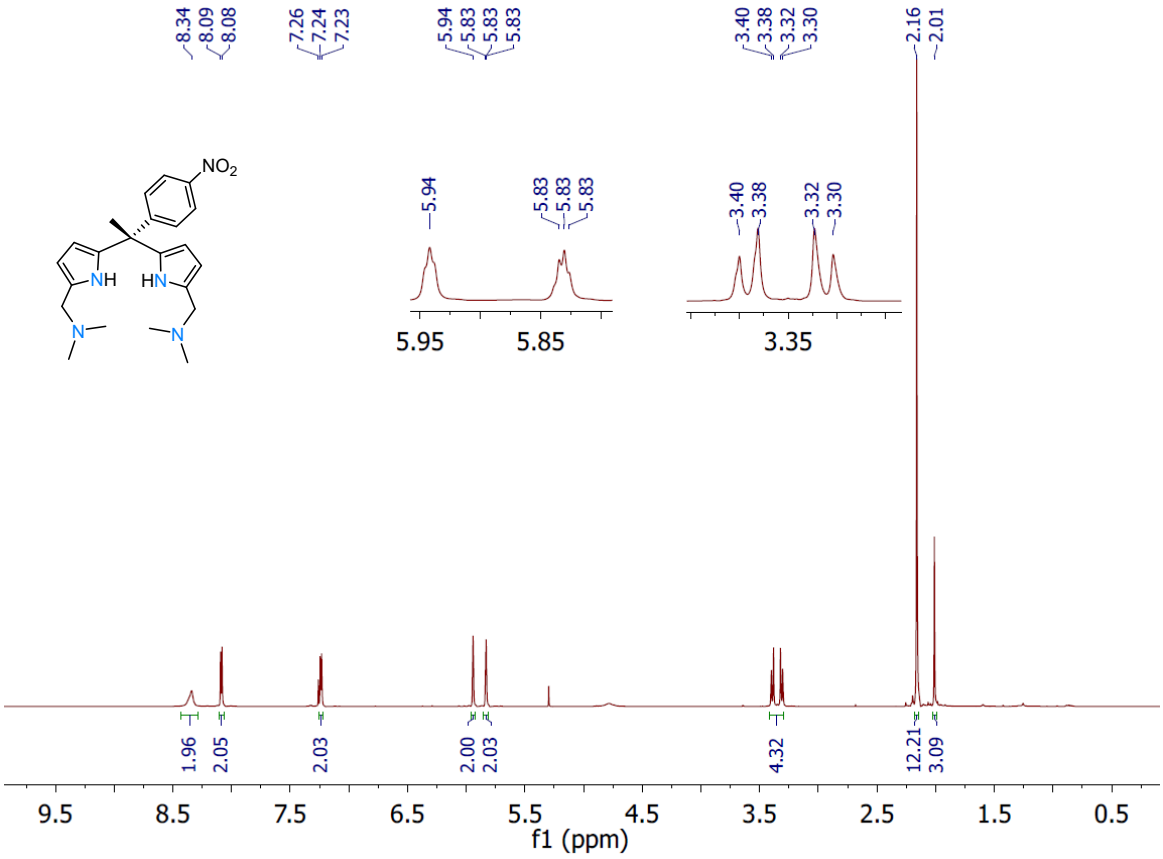

Figure S6: ^{1}H NMR (700 MHz) spectrum of **2c** in $CDCl_3$ at room temperature.

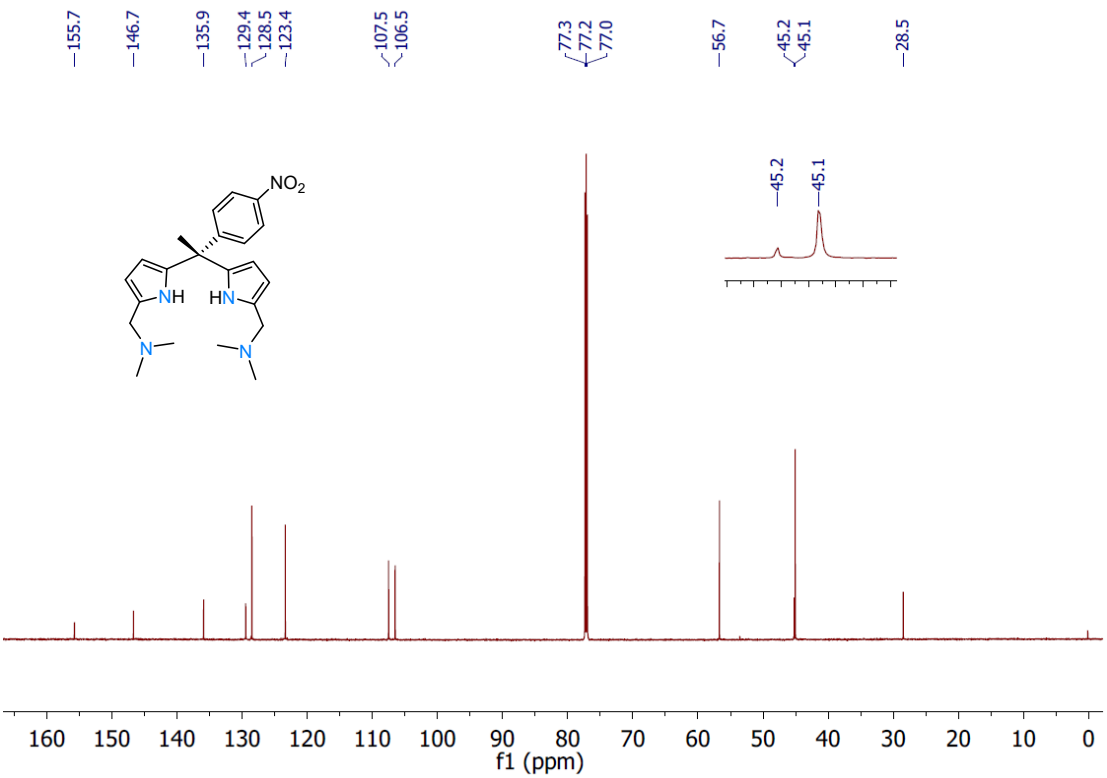

Figure S7: $^{13}C\{^{1}H\}$ NMR (175 MHz) spectrum of **2c** in $CDCl_3$ at room temperature.

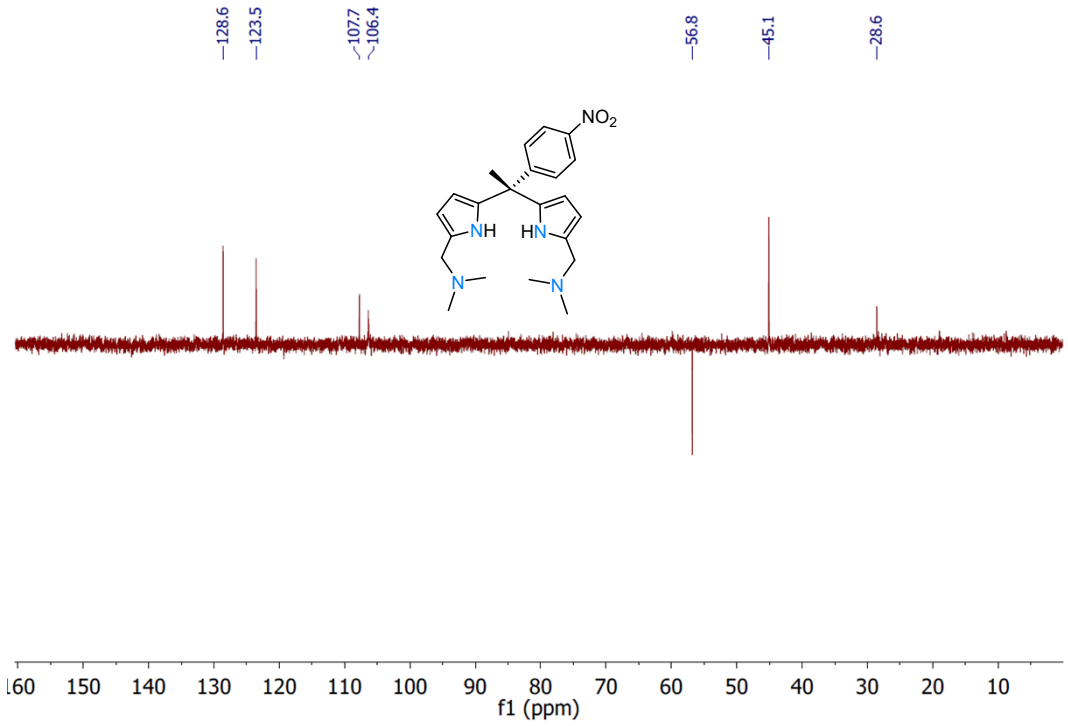

Figure S8: DEPT-135$\{^{1}H\}$ NMR (175 MHz) spectrum of **2c** in $CDCl_3$ at room temperature.

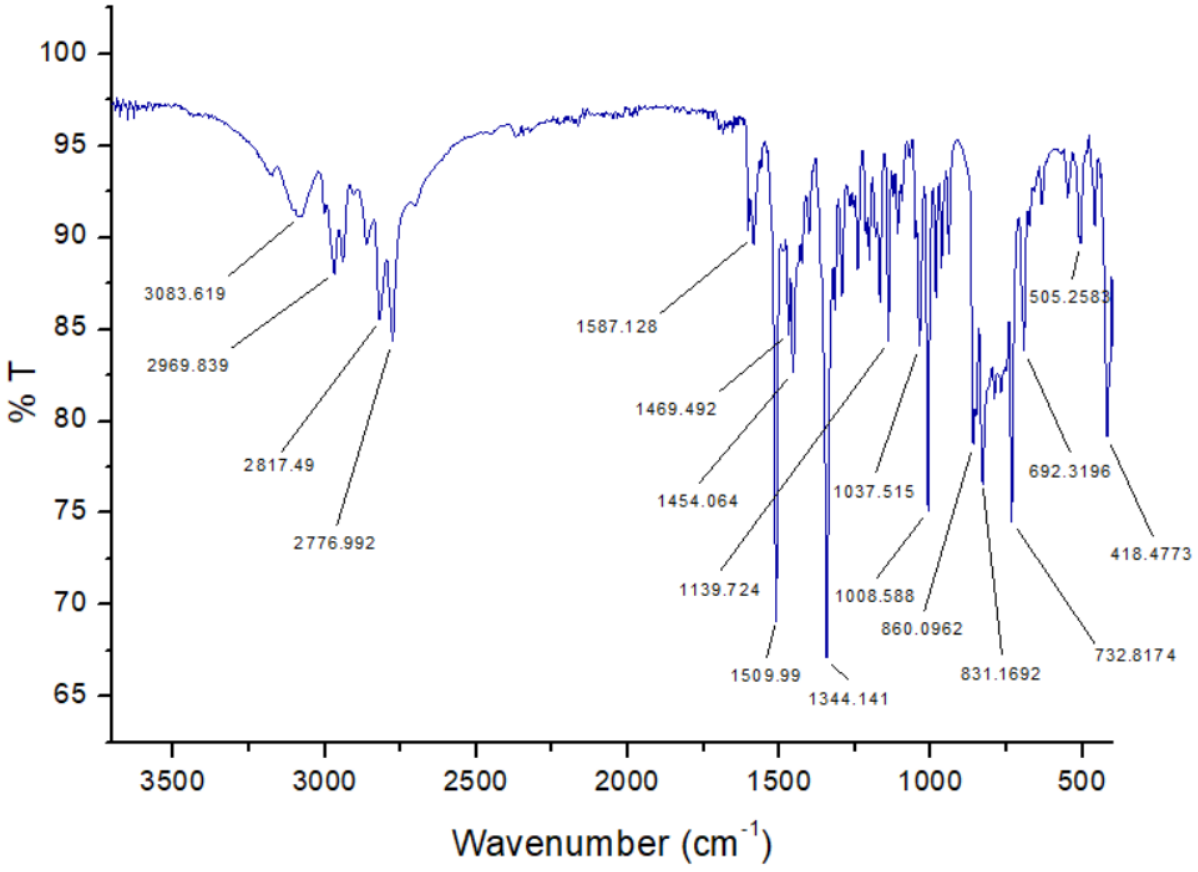

Figure S9: ATR spectrum of **2c**.

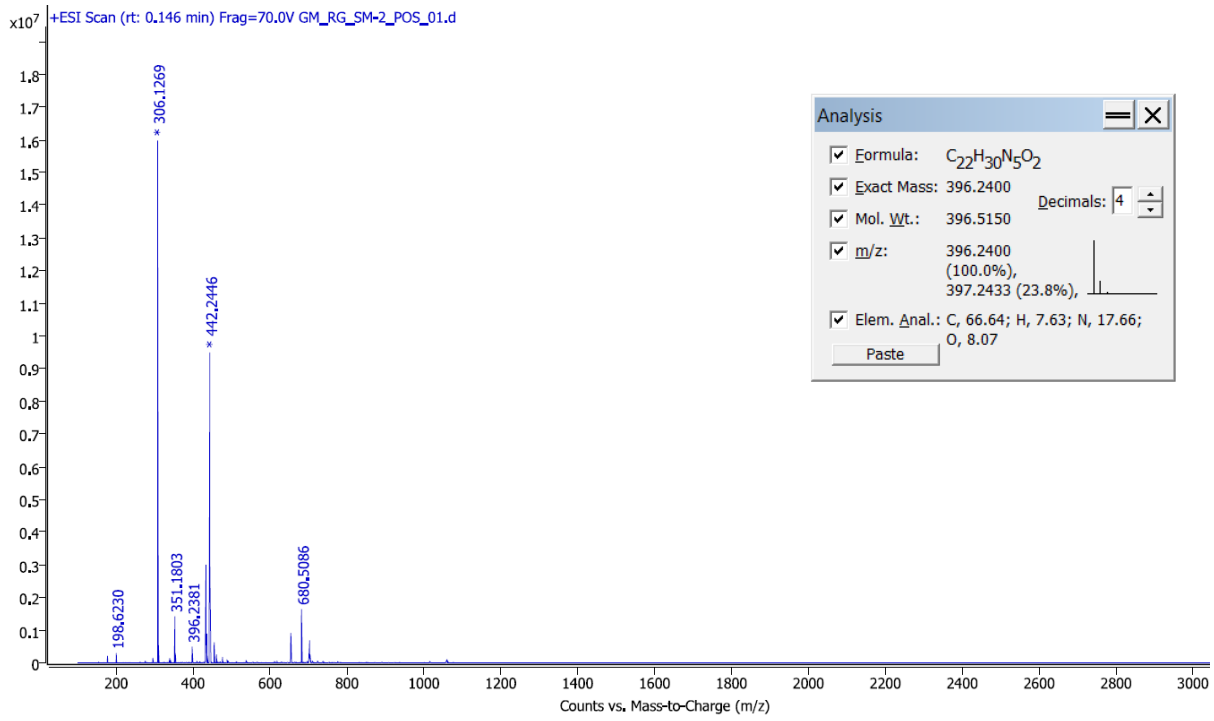

Figure S10: HRMS (ESI+) spectrum of **2c**, showing $[M+H]^+$ peak at 396.2381 (calcd: 396.2400).

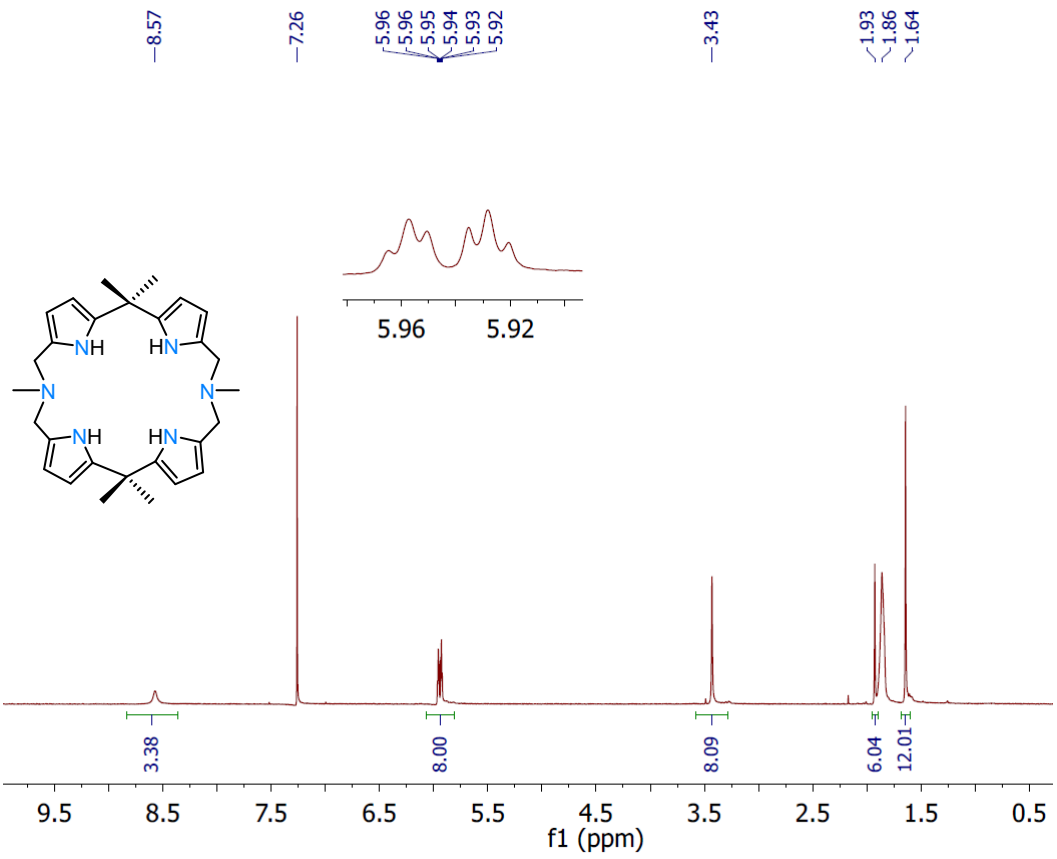

Figure S11: ^{1}H NMR (400 MHz) spectrum of **3a** in $CDCl_3$ at room temperature.

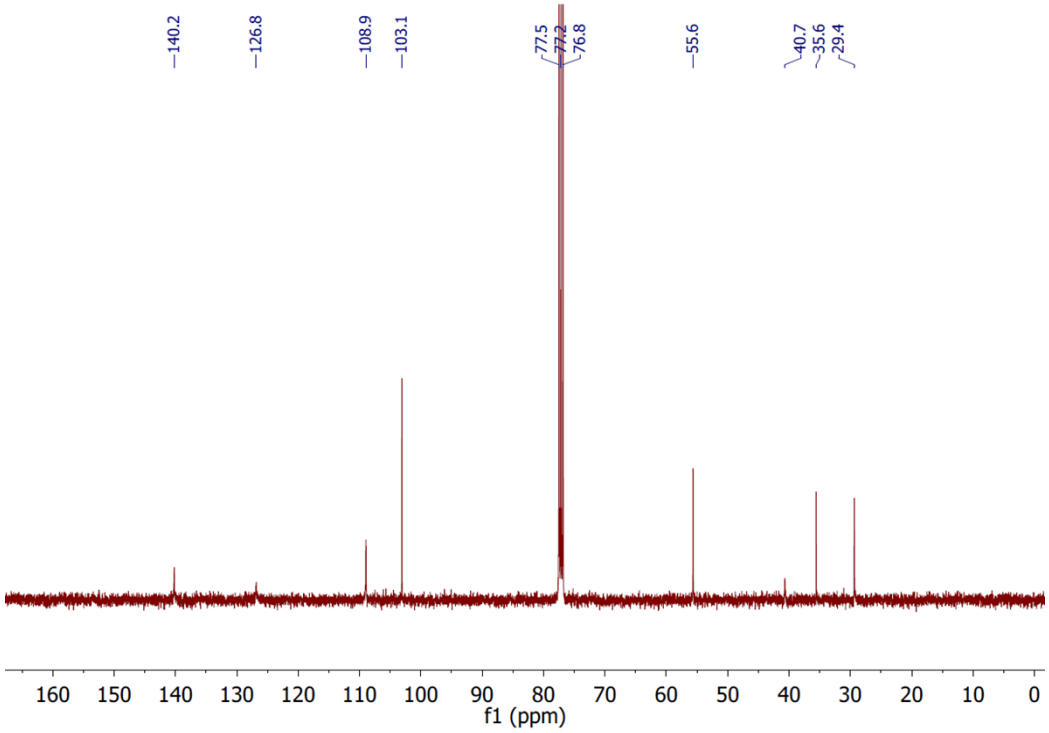

Figure S12: $^{13}C\{^{1}H\}$ NMR (100 MHz) spectrum of **3a** in $CDCl_3$ at room temperature.

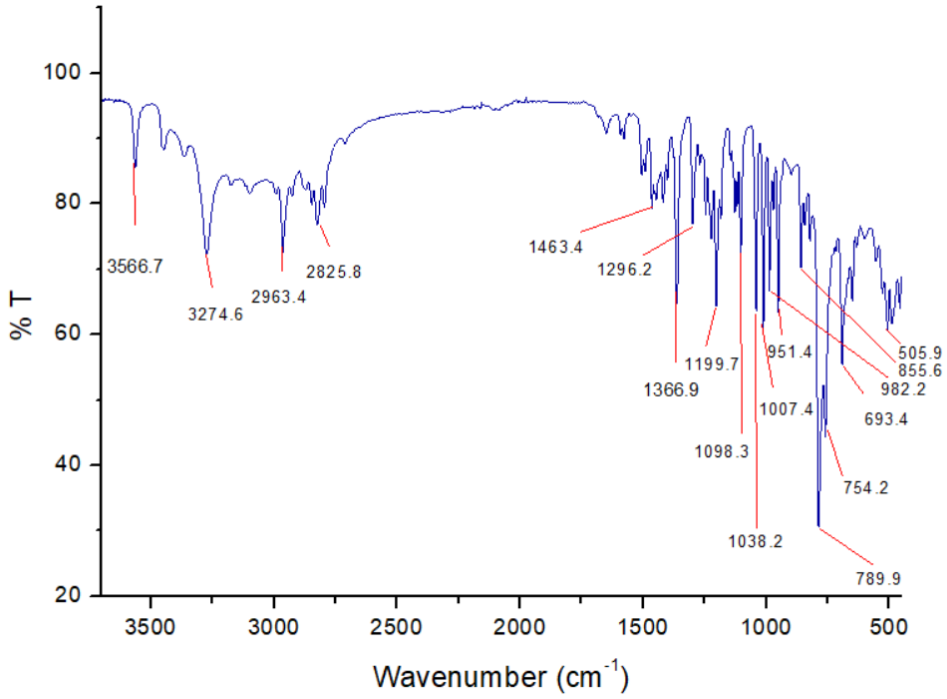

Figure S13: ATR spectrum of **3a**.

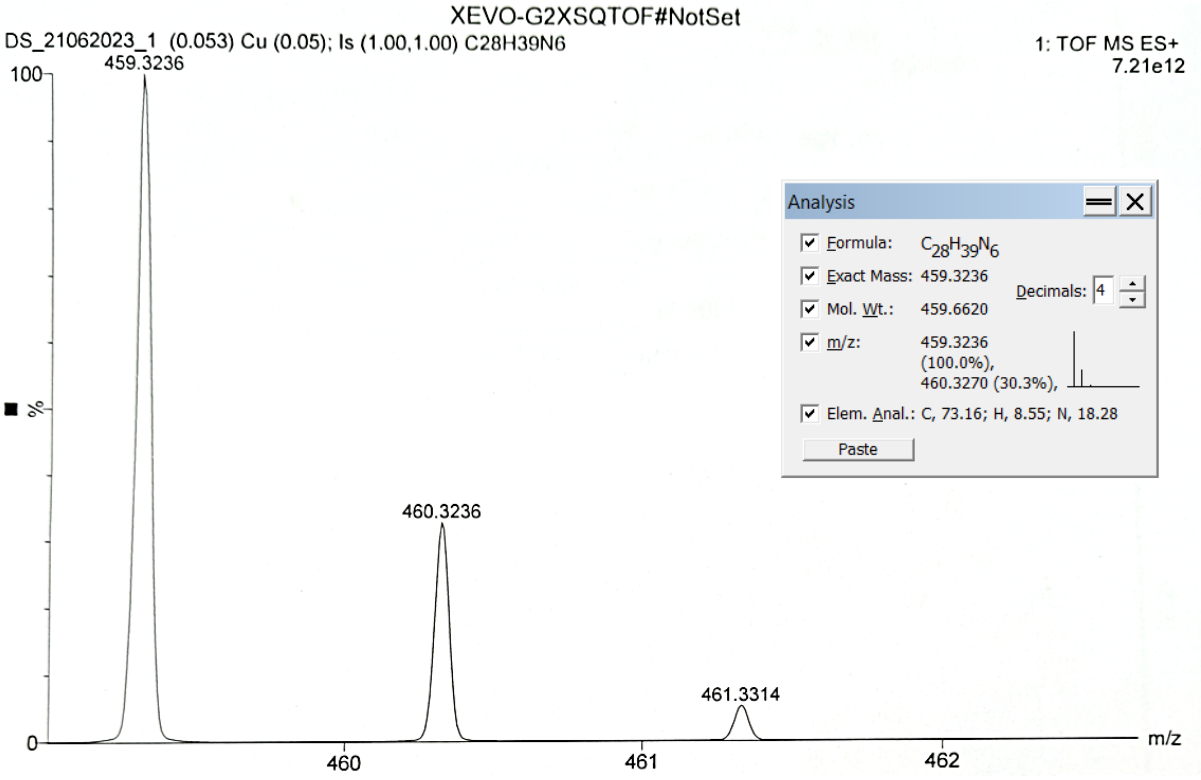

Figure S14: HRMS (ESI+) spectrum of **3a**, showing $[M+H]^+$ peak at 459.3236 (calcd: 459.3236).

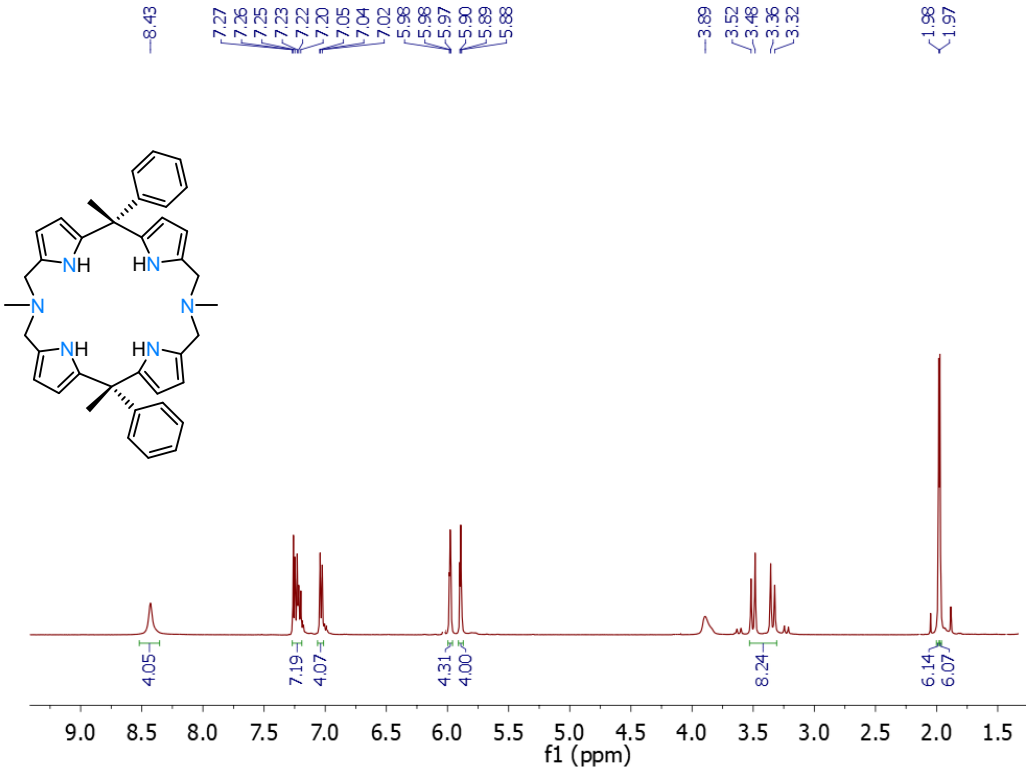

Figure S15: ^{1}H NMR (400 MHz) spectrum of **3b** in $CDCl_3$ at room temperature.

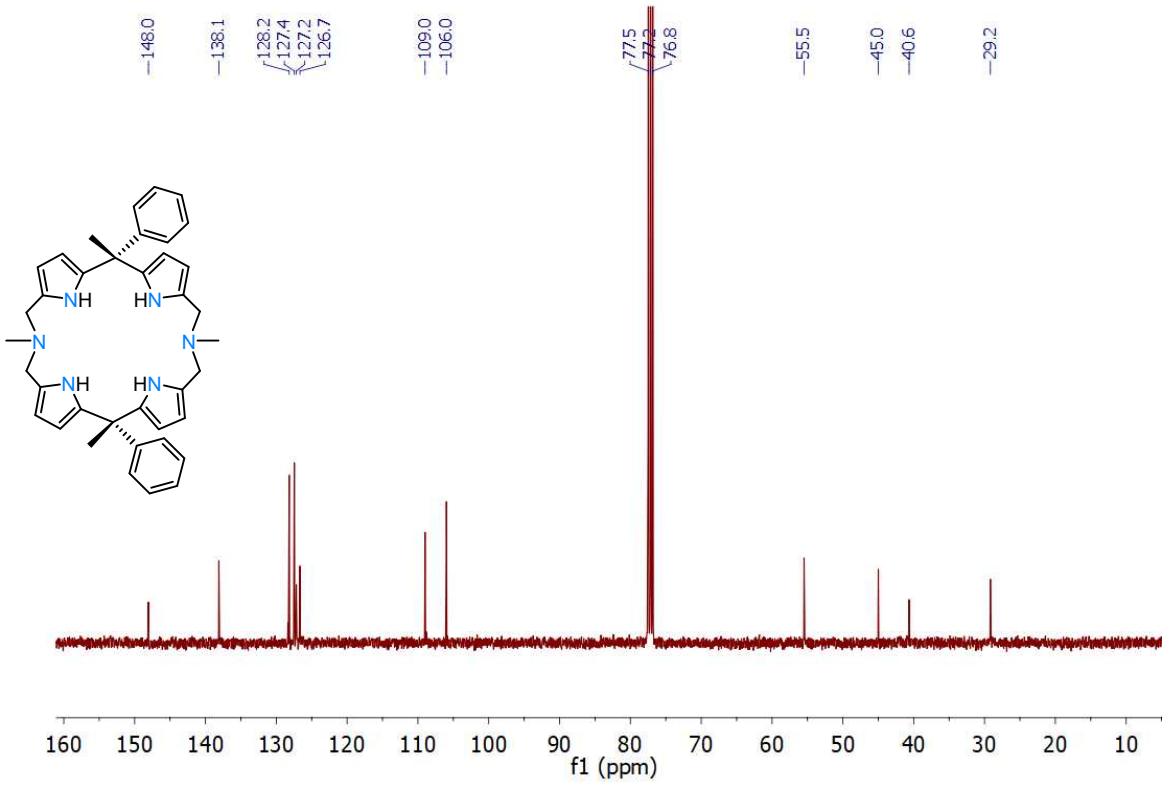

Figure S16: $^{13}C\{^{1}H\}$ NMR (100 MHz) spectrum of **3b** in $CDCl_3$ at room temperature.

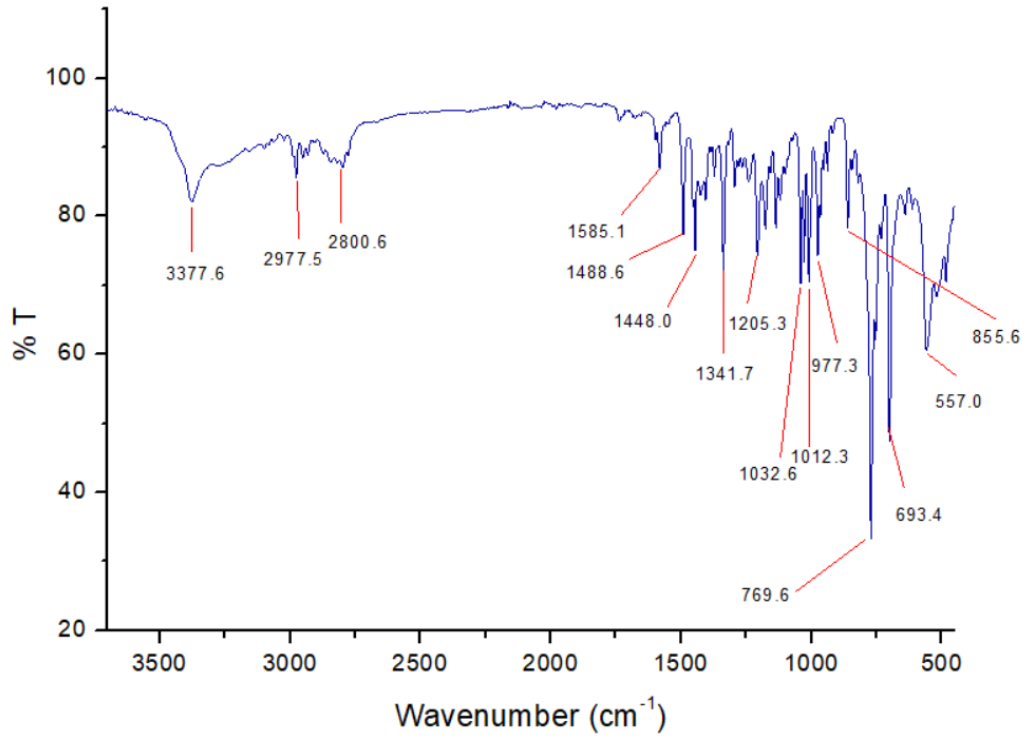

Figure S17: ATR spectrum of **3b**.

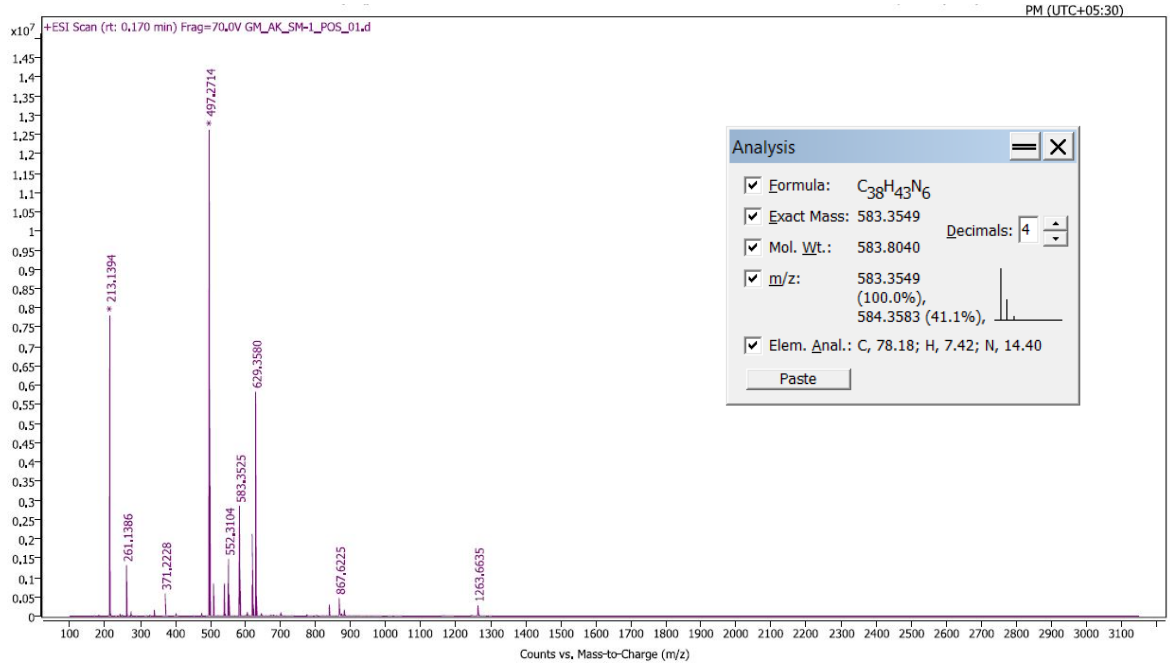

Figure S18: HRMS (ESI+) spectrum of **3b**, showing $[M+H]^+$ peak at 583.3525 (calcd: 583.3549).

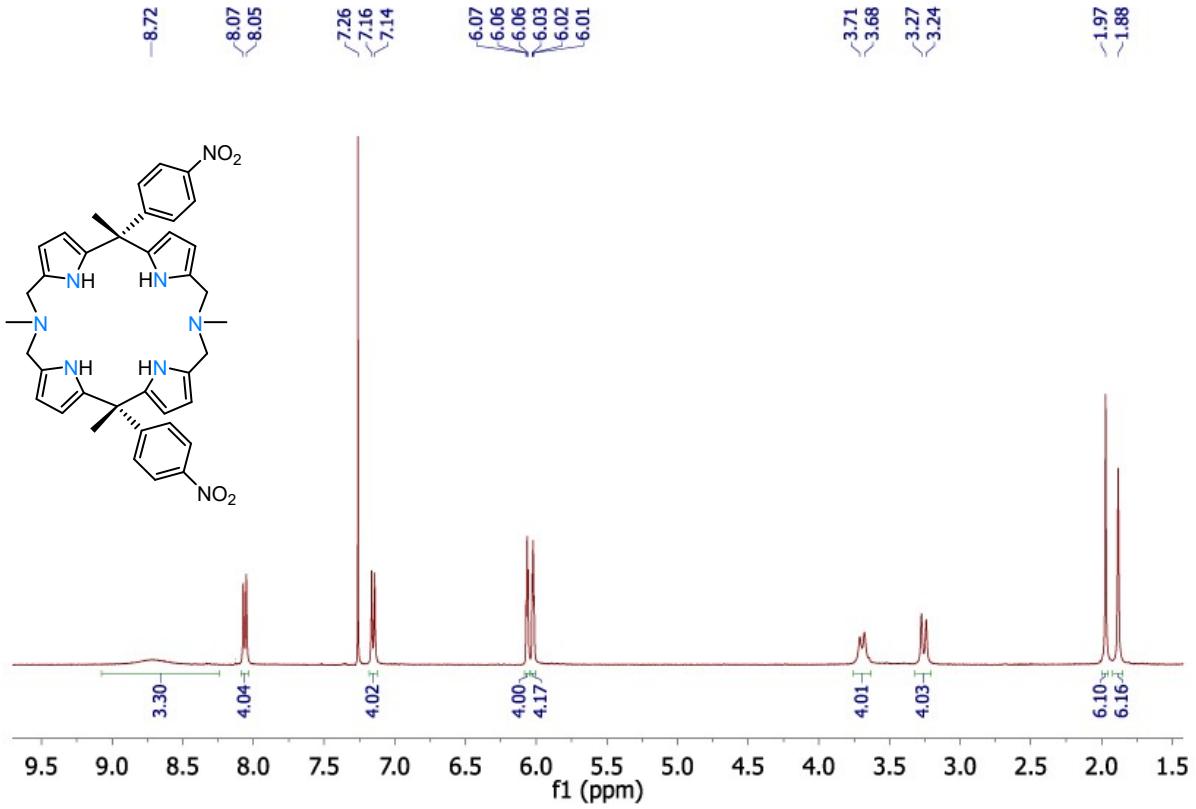

Figure S19: ^{1}H NMR (400 MHz) spectrum of **3c** in $CDCl_3$ at room temperature.

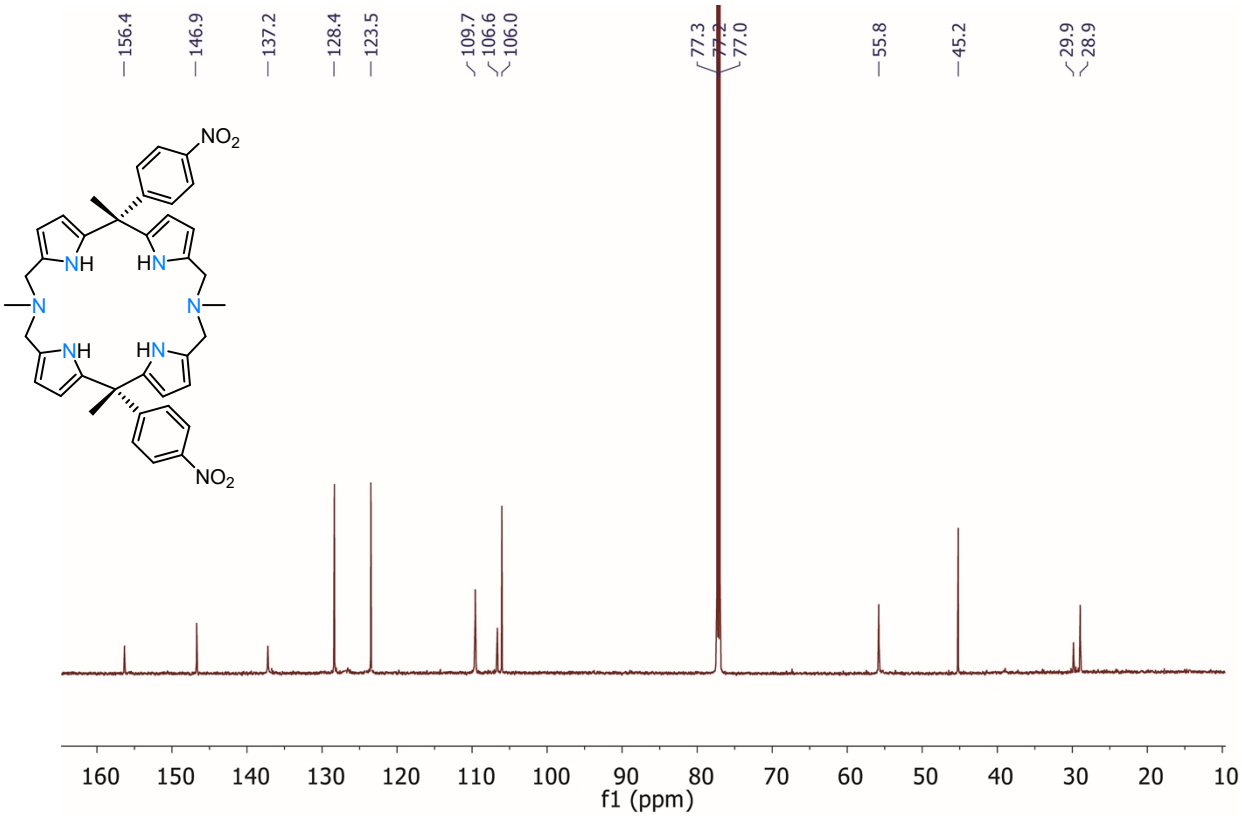

Figure S20: $^{13}C\{^{1}H\}$ NMR (175 MHz) spectrum of **3c** in $CDCl_3$ at room temperature.

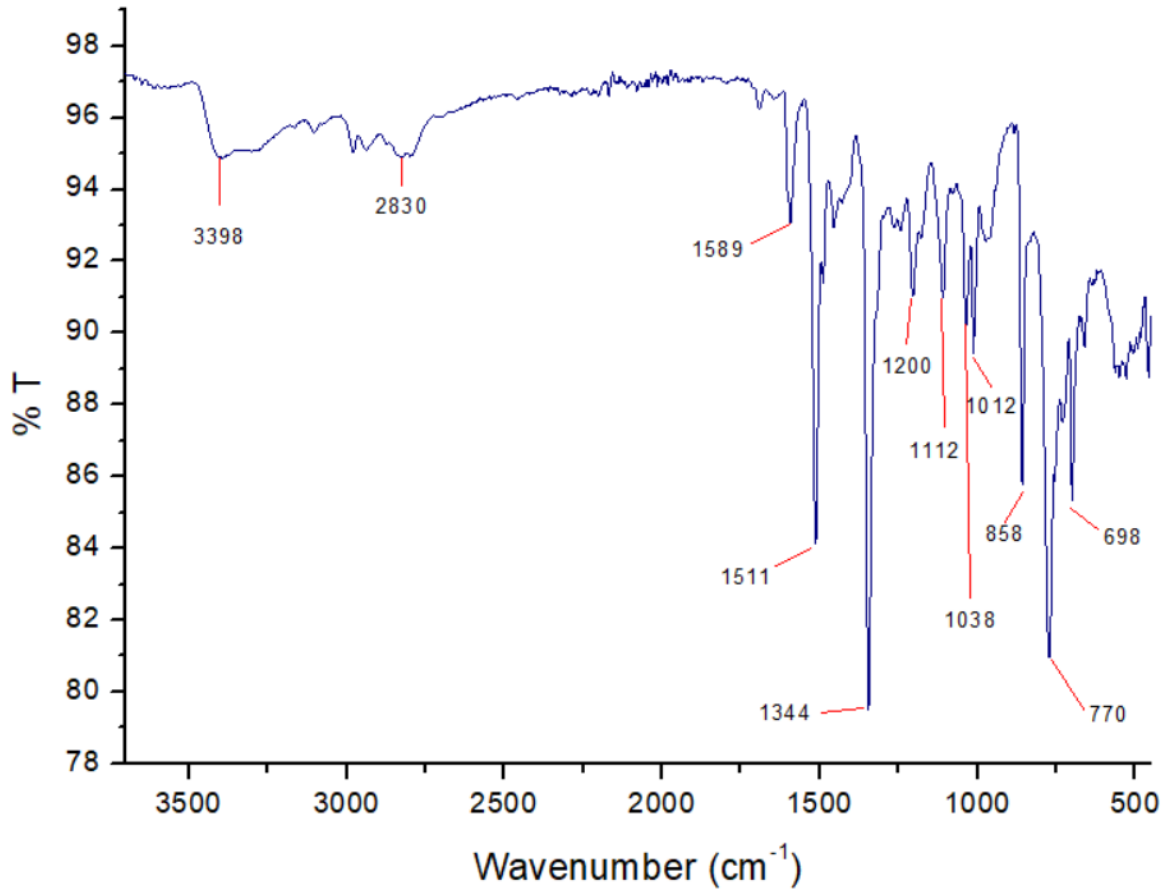

Figure S21: ATR spectrum of **3c**.

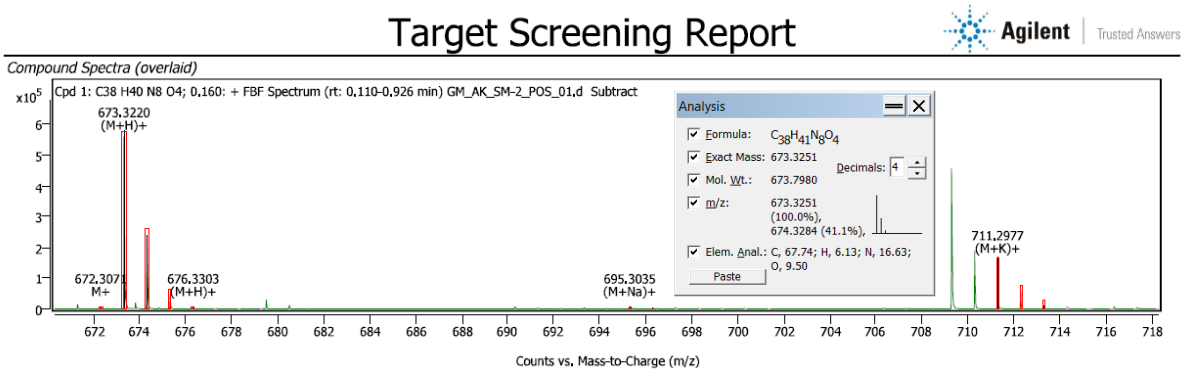

Figure S22: HRMS (ESI+) spectrum of **3c**, showing $[M+H]^+$ peak at 673.3220 (calcd: 673.3251).

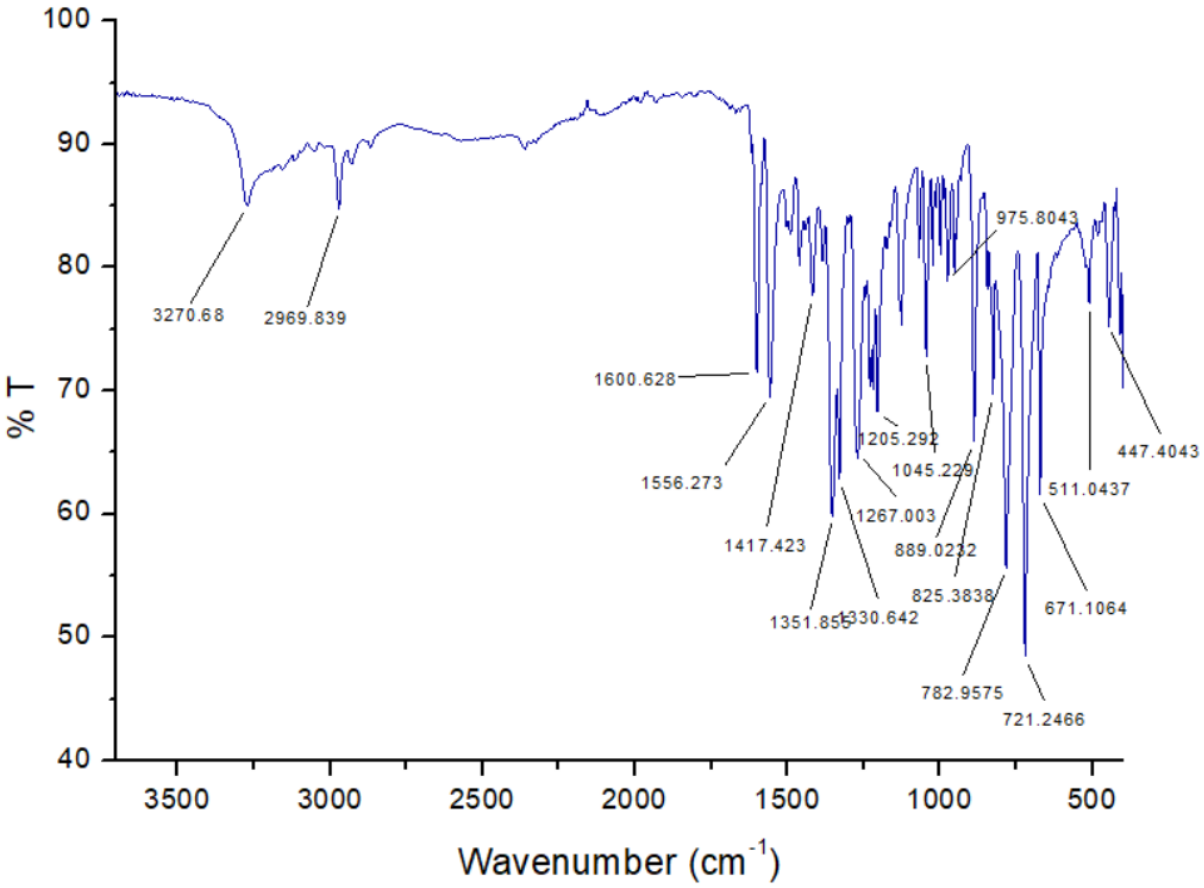

Figure S23: ATR spectrum of benzoate complex $[\mathbf{3a}H_2]^{2+}[PhCOO^-]_2$.

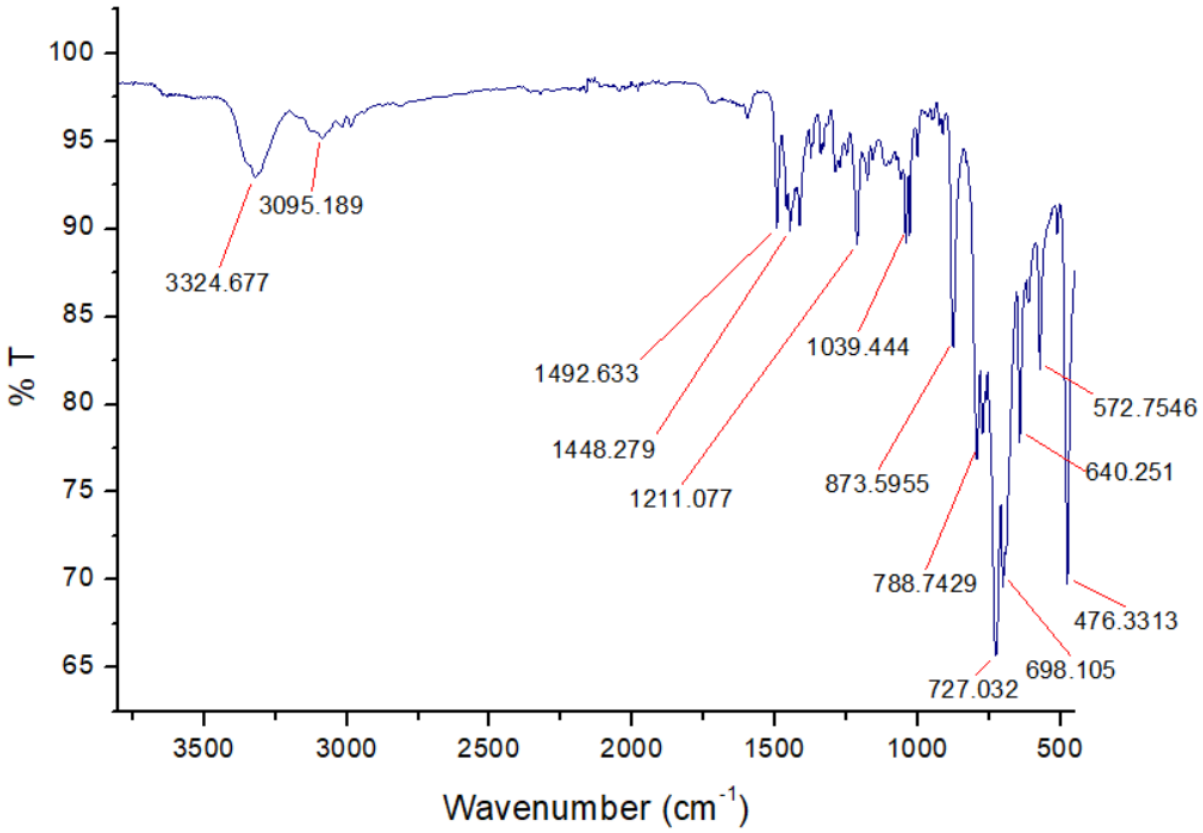

Figure S24: ATR spectrum of hexafluorosilicate complex [**3b**H_2]$^{2+}$[SiF_6^{2-}].

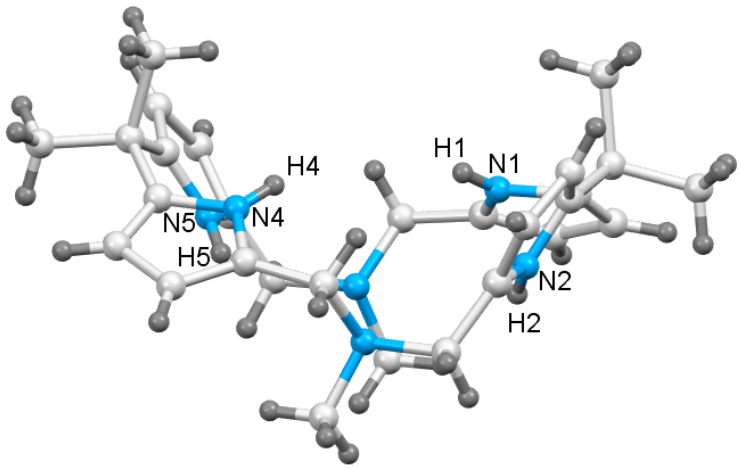

Figure S25: X-ray structure of **3a**, showing the 1,3-*alternate* conformation of the macrocycle. Lattice water molecules are omitted for clarity.

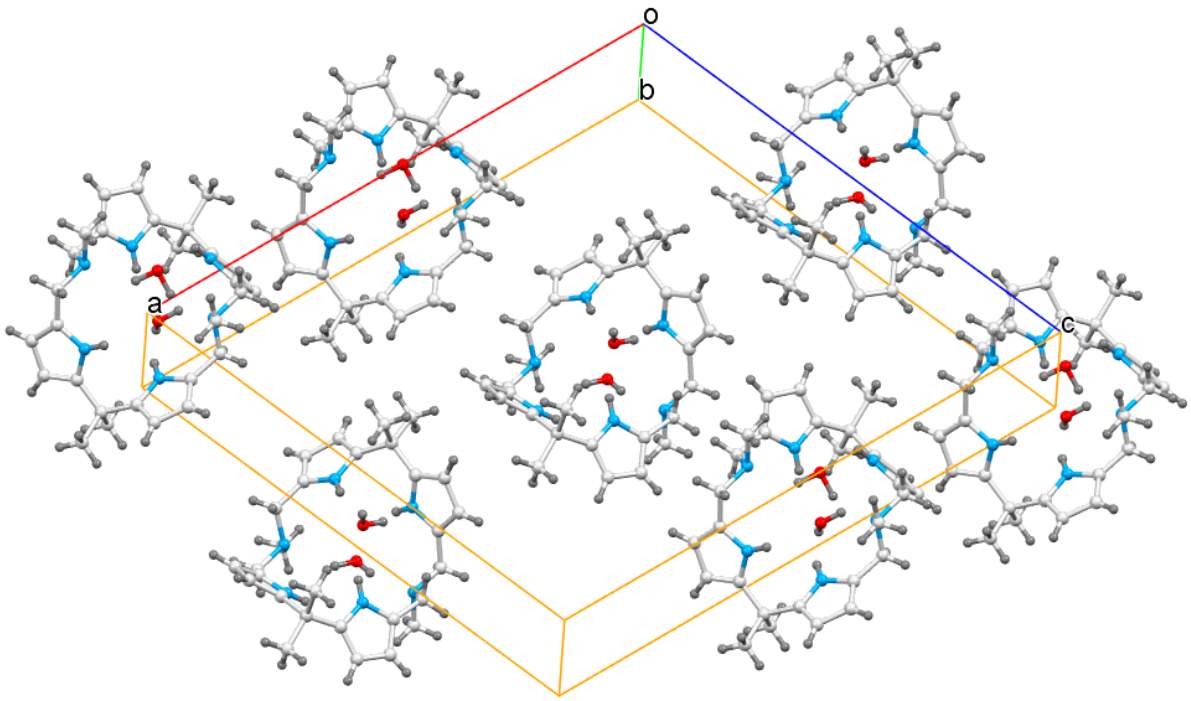

Figure S26: Unit cell packing diagram of **3a**.

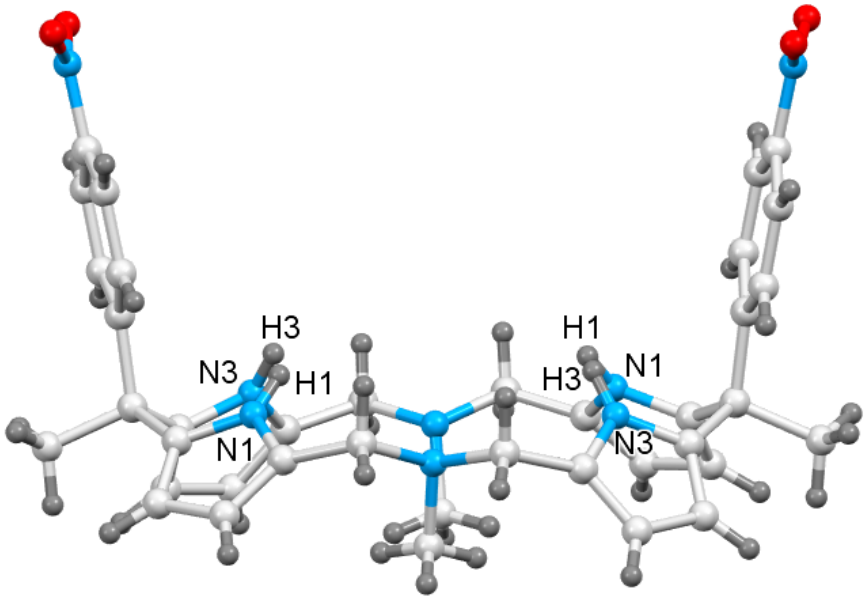

Figure S27: X-ray structure of **3c**, showing the cone conformation of the macrocycle. Lattice water molecule is omitted for clarity.

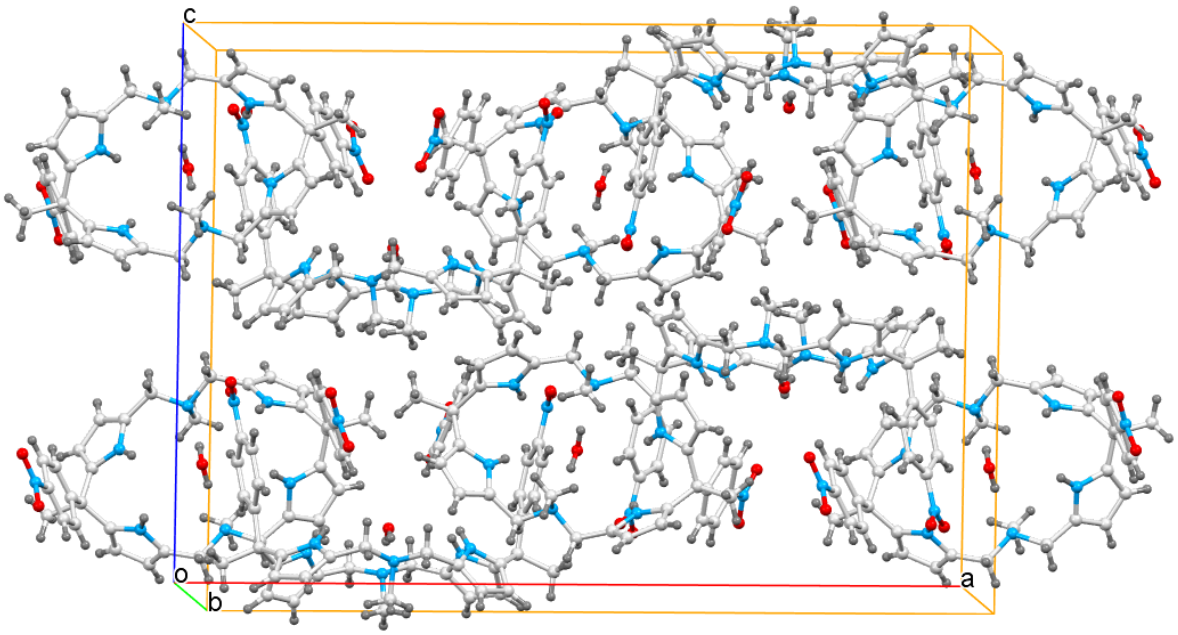

Figure S28: Unit cell packing diagram of **3c**.

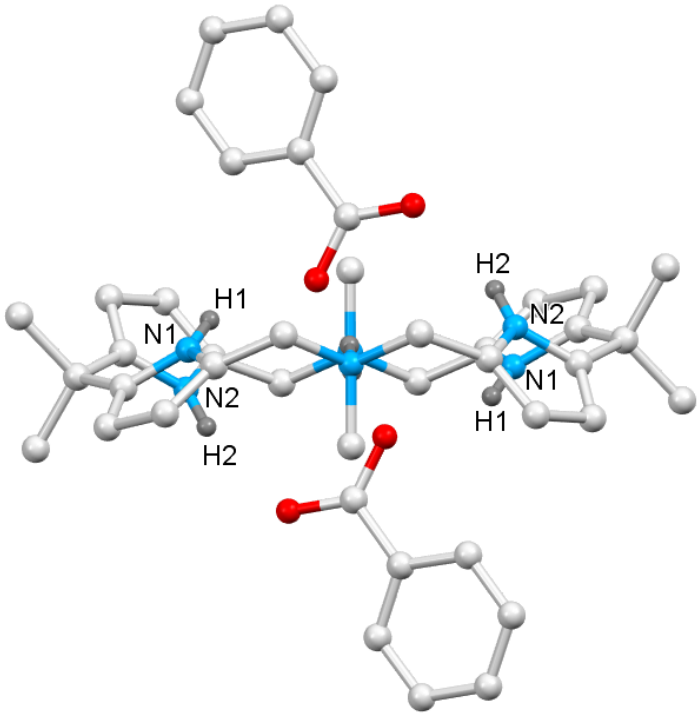

Figure S29: X-ray structure of $[\mathbf{3a}H_2]^{2+}[PhCOO^-]_2$, showing the 1,2-*alternate* conformation of the macrocycle.

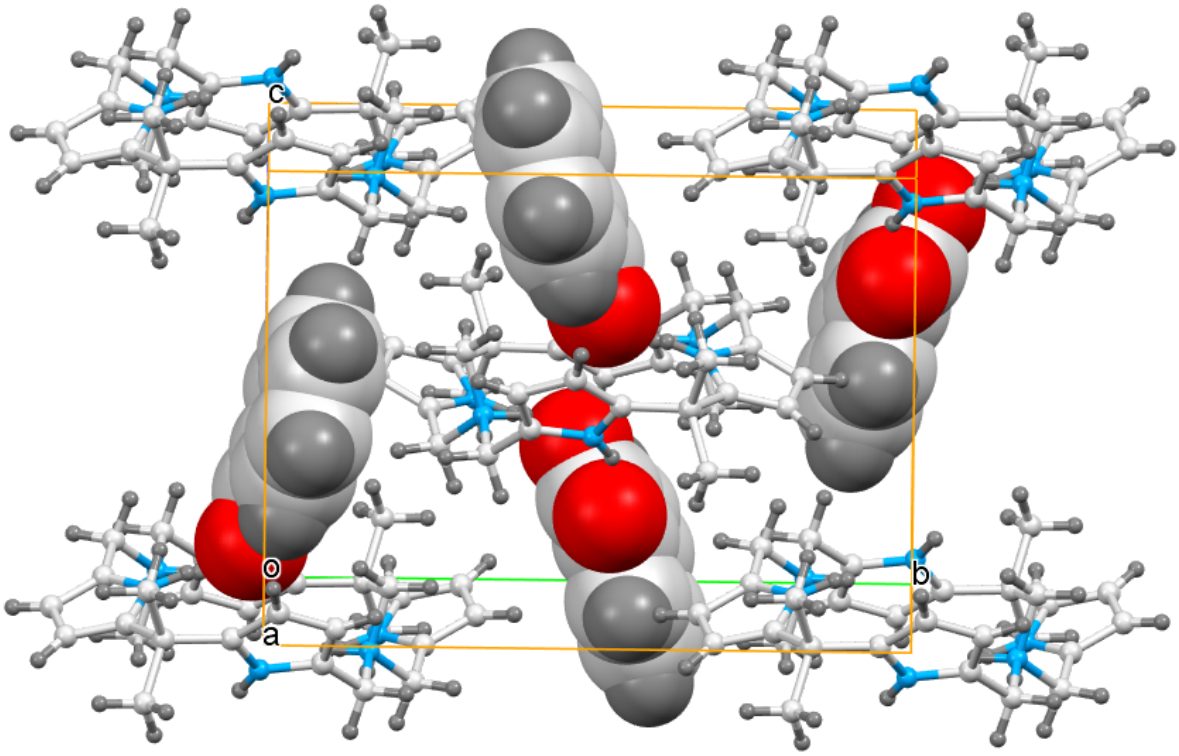

Figure S30: Unit cell packing diagram of $[\mathbf{3a}H_2]^{2+}[PhCOO^-]_2$.

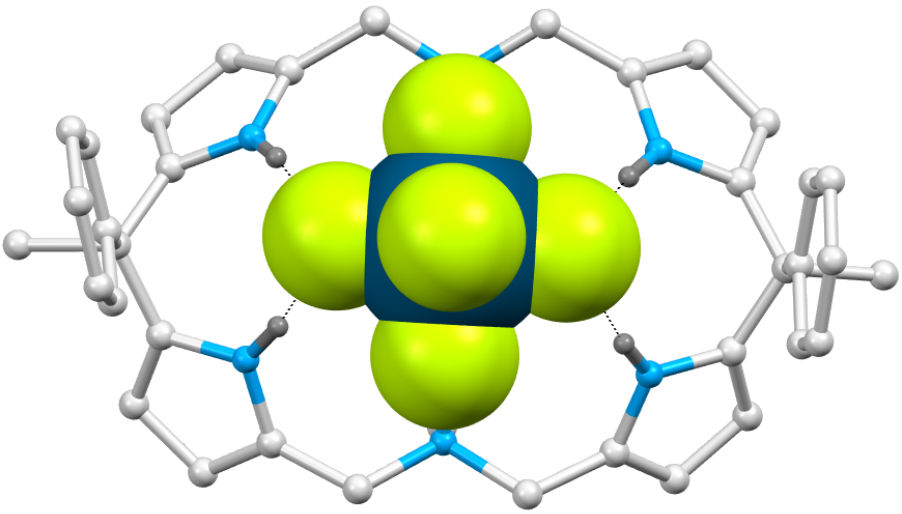

Figure S31: X-ray structure of $[\mathbf{3b}H_2]^{2+}[SiF_6^{2-}]$ (front view), showing the cone conformation of the macrocycle. Disordered fluorine atoms are not shown.

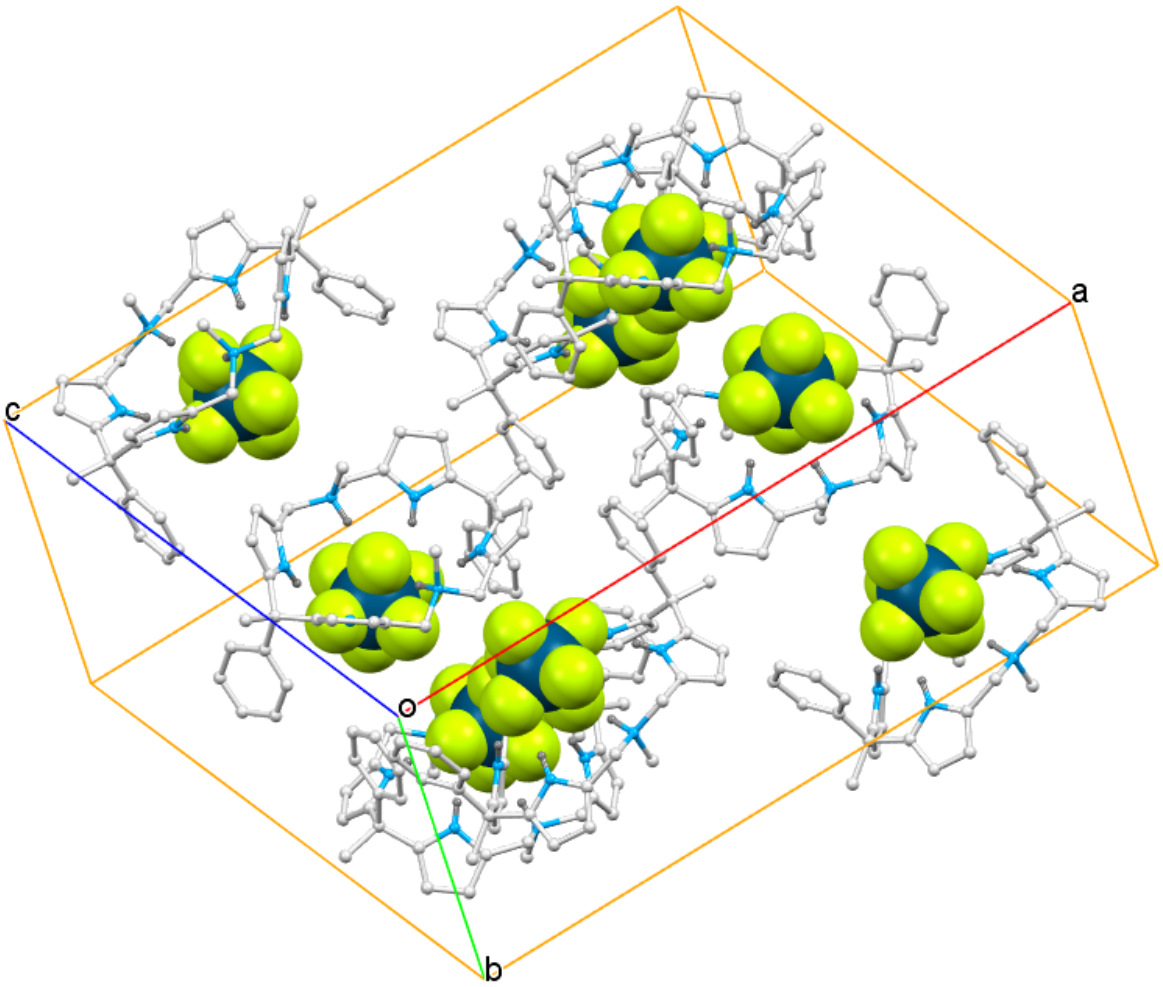

Figure S32: Unit cell packing diagram of $[\mathbf{3b}H_2]^{2+}[SiF_6^{2-}]$.

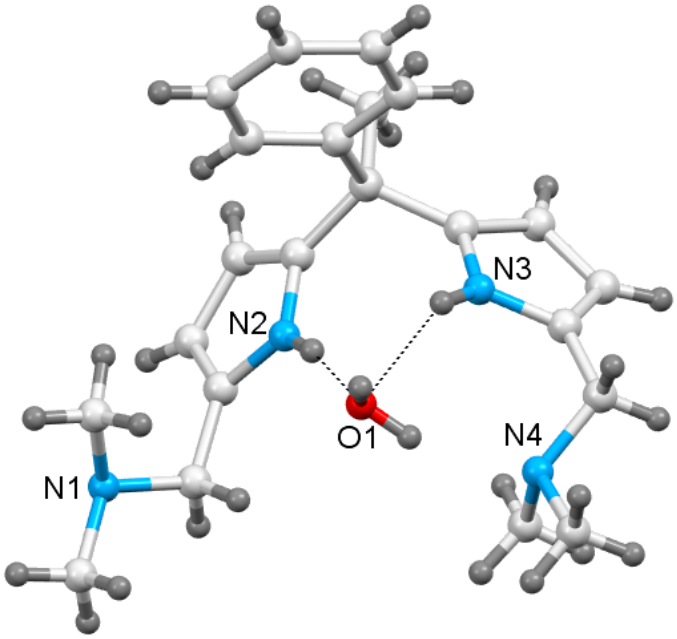

Figure S33: X-ray structure of **2b**, showing one lattice water molecule is hydrogen-bonded to the pyrrolic NH protons. The crystal data is poor to get reliable structural parameters.

UV-visible titrations:

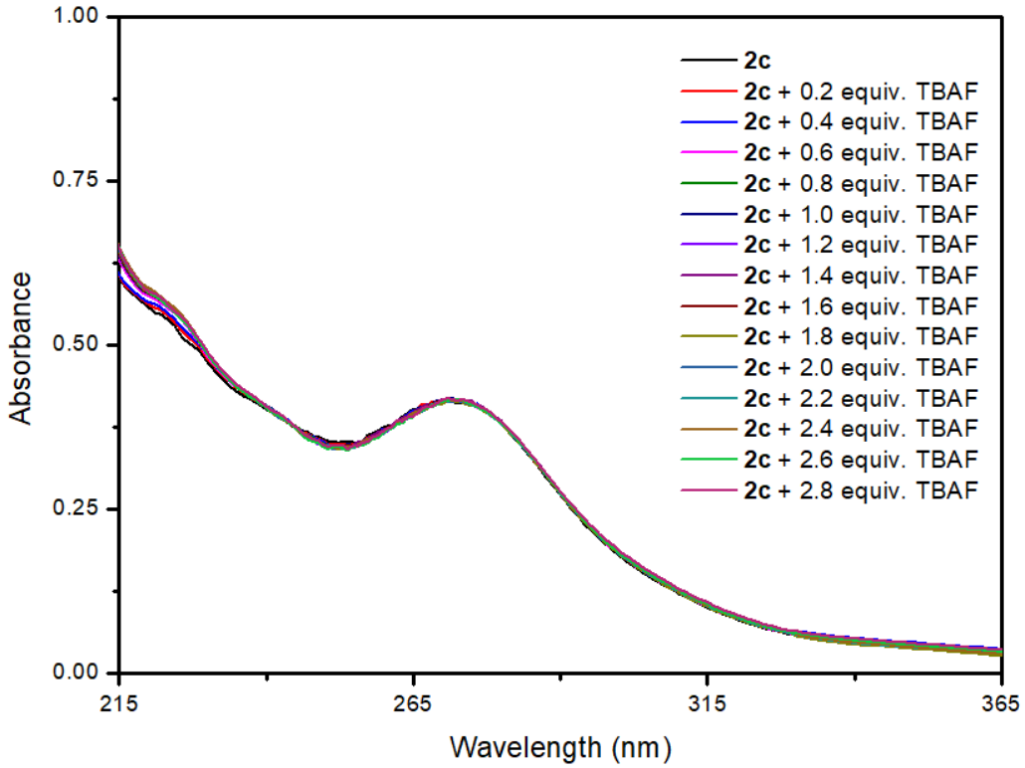

Figure S34: UV-vis spectrum of receptor **2c** (10^{-5} M in CH_3CN) observed upon the incremental addition of TBAF (10^{-3} M in CH_3CN).

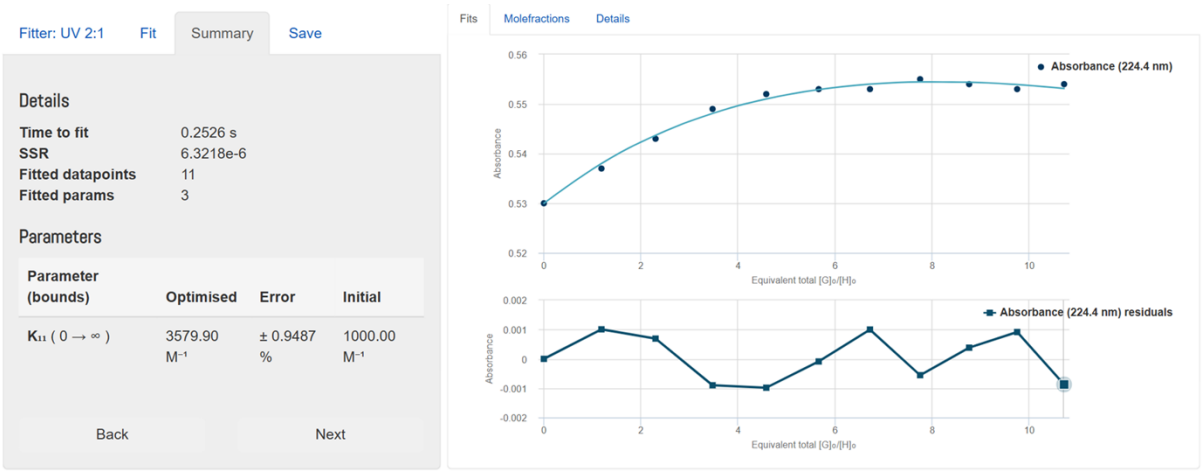

Figure S35: UV-vis absorbance titration data (at 224.4 nm) of receptor **2c** (10^{-5} M) observed upon the addition of TBAF (10^{-3} in CH_3CN) and fitted to 2:1 (H:G) binding model of BindFit v0.5.

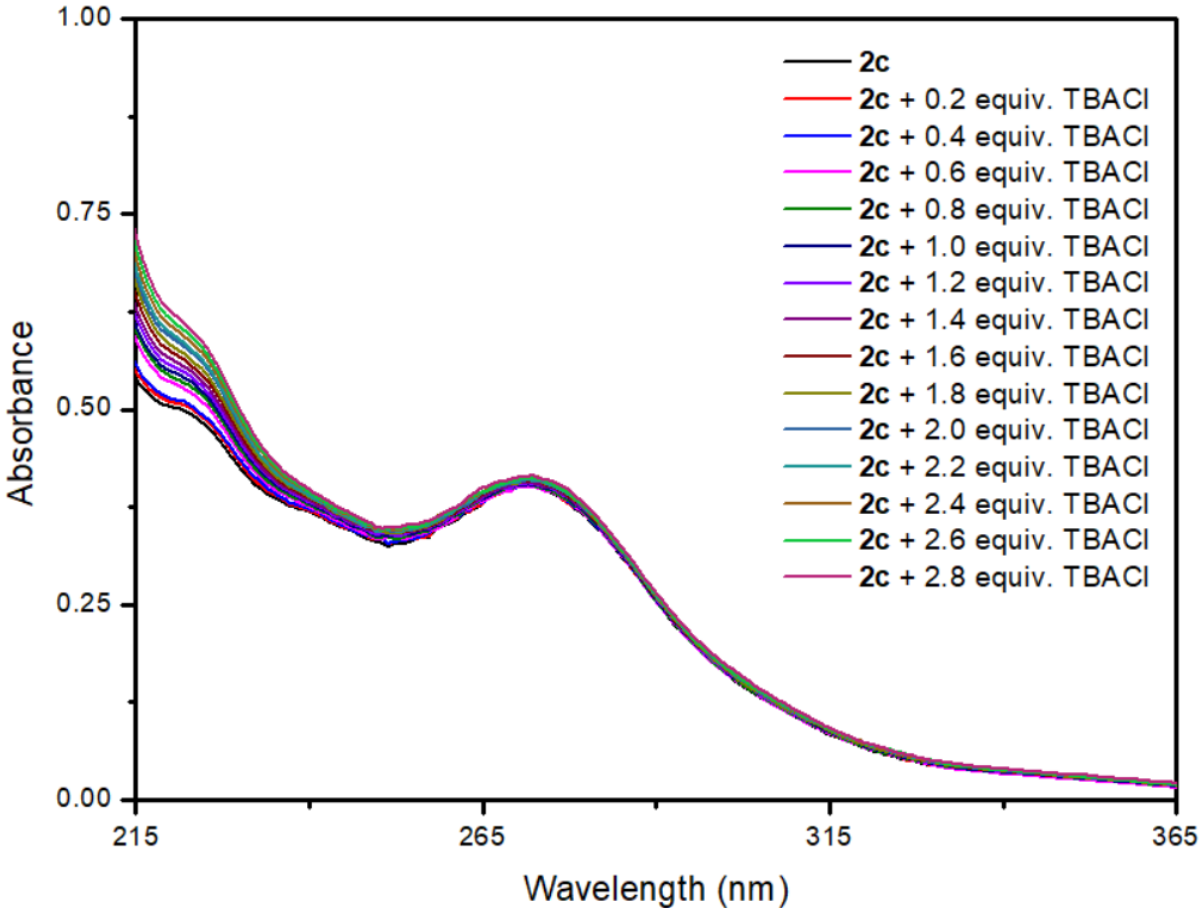

Figure S36: UV-vis spectrum of receptor **2c** (10^{-5} M in CH_3CN) observed upon the incremental addition of TBACl (10^{-3} M in CH_3CN).

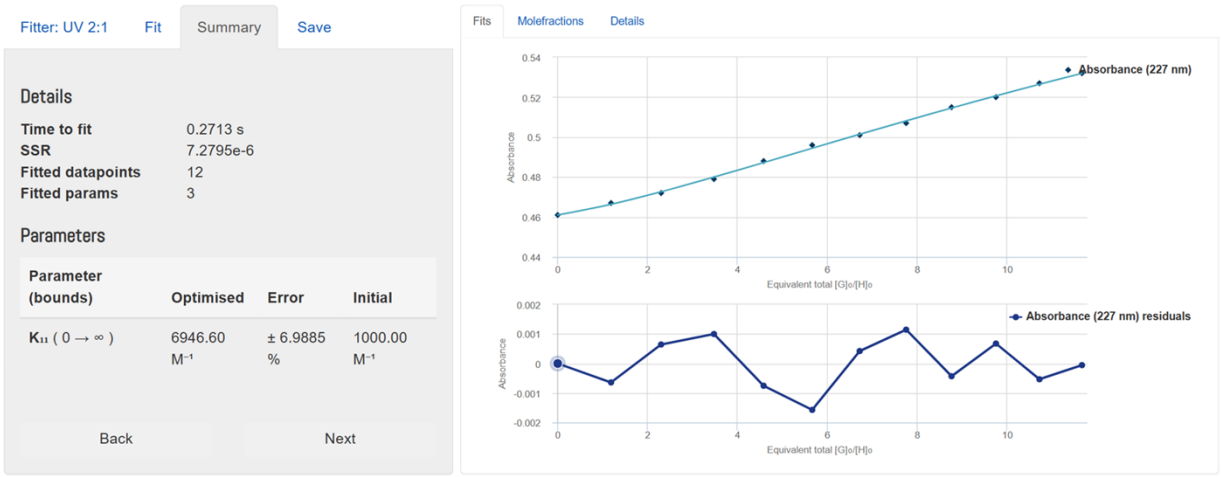

Figure S37: UV-vis absorbance titration data (at 227 nm) of receptor **2c** (10^{-5} M) observed upon the addition of TBACl (10^{-3} in CH_3CN) and fitted to 2:1 (H:G) binding model of BindFit v0.5.

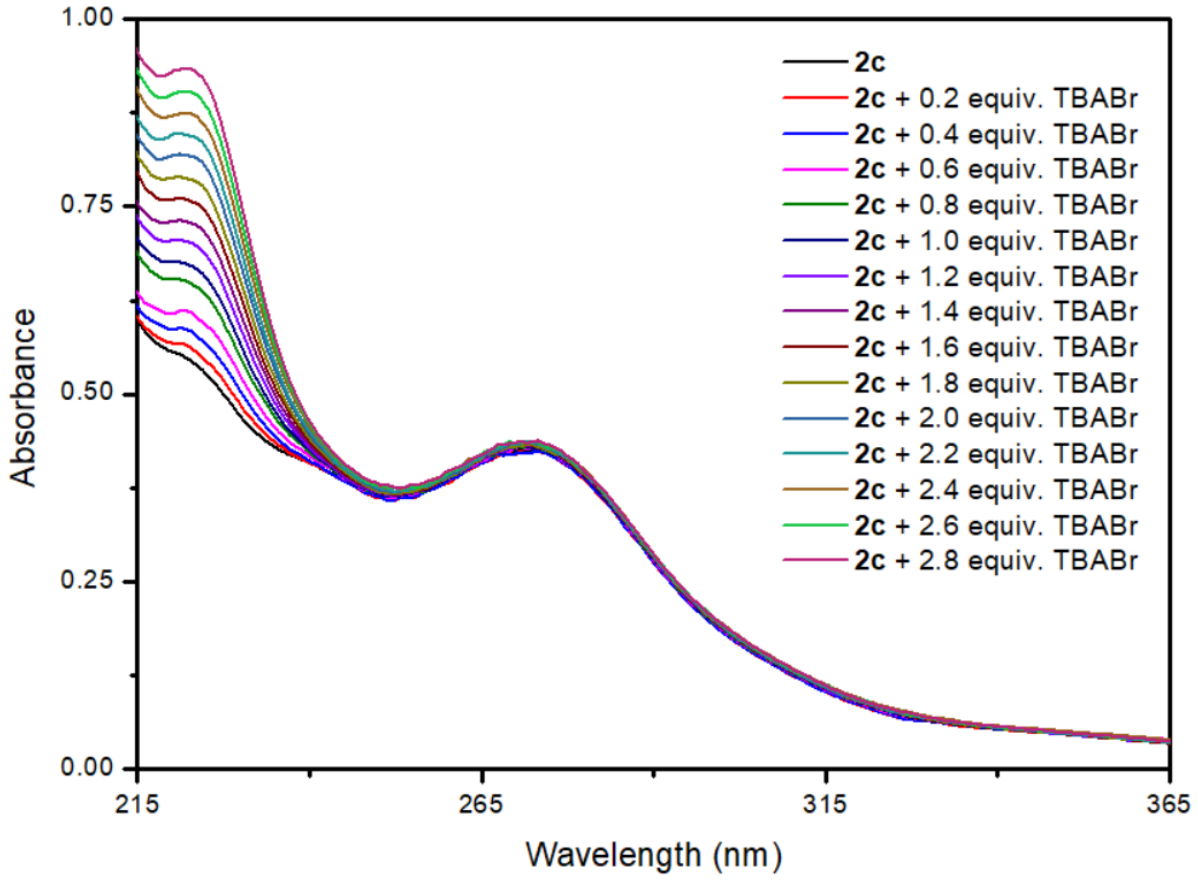

Figure S38: UV-vis spectrum of receptor **2c** (10^{-5} M in CH_3CN) observed upon the incremental addition of TBABr (10^{-3} M in CH_3CN).

Figure S39: UV-vis absorbance titration data (at 232 nm) of receptor **2c** (10^{-5} M) observed upon the addition of TBABr (10^{-3} in CH_3CN) and fitted to 2:1 (H:G) binding model of BindFit v0.5.

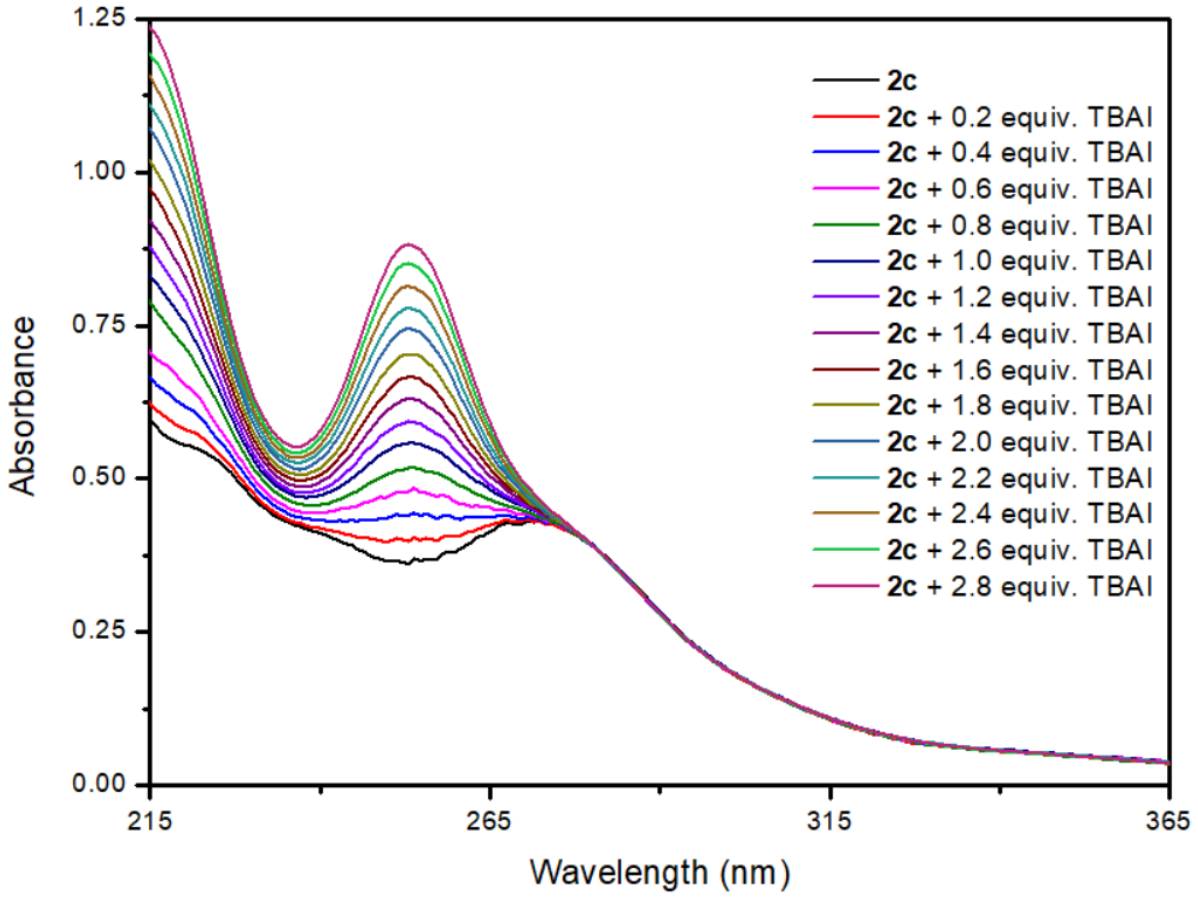

Figure S40: UV-vis spectrum of receptor **2c** (10^{-5} M in CH_3CN) observed upon the incremental addition of TBAI (10^{-3} M in CH_3CN).

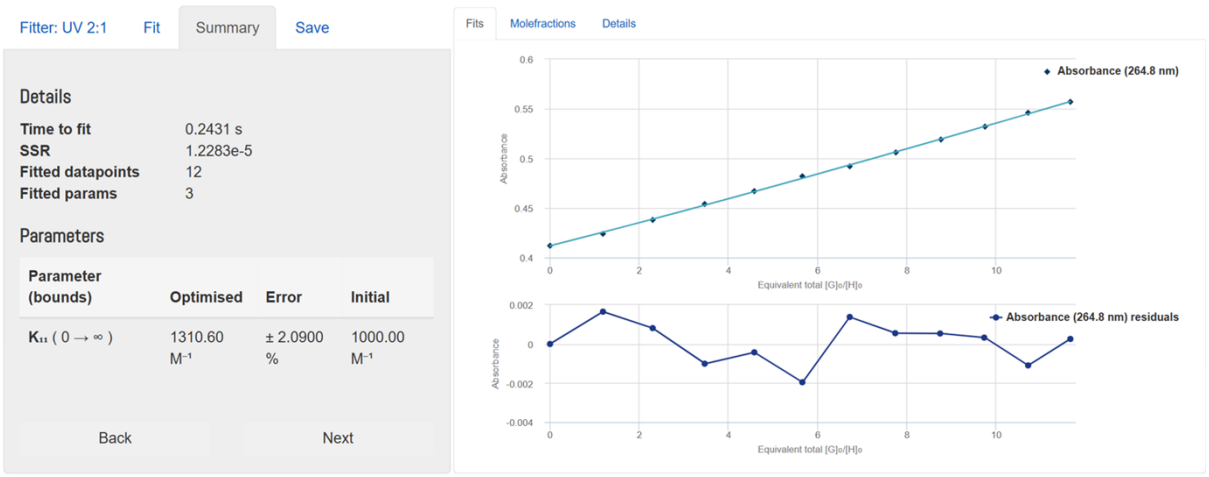

Figure S41: UV-vis absorbance titration data (at 264.8 nm) of receptor **2c** (10^{-5} M) observed upon the addition of TBAI (10^{-3} in CH_3CN) and fitted to 2:1 (H:G) binding model of BindFit v0.5.

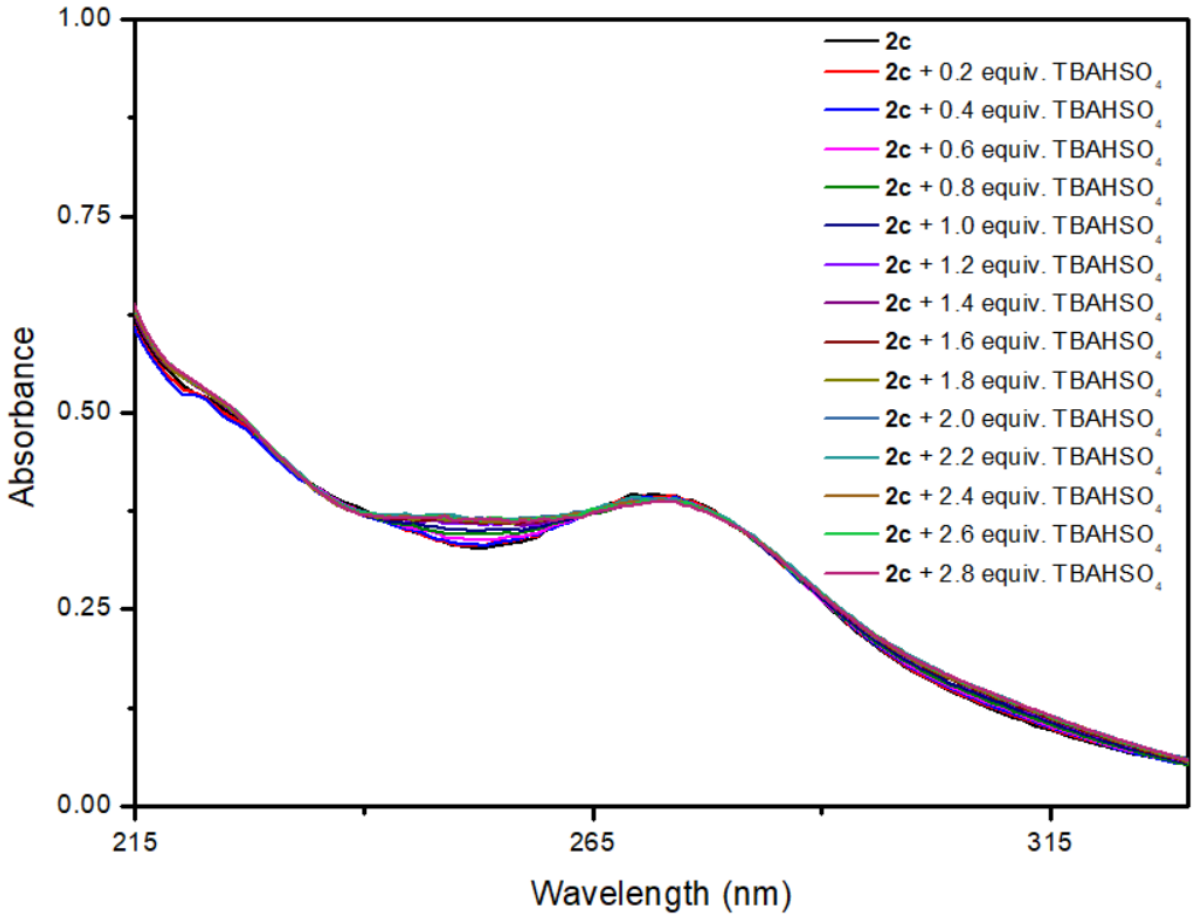

Figure S42: UV-vis spectrum of receptor **2c** (10^{-5} M in CH_3CN) observed upon the incremental addition of $TBAHSO_4$ (10^{-3} M in CH_3CN).

Figure S43: UV-vis absorbance titration data (at 260.6 nm) of receptor **2c** (10^{-5} M) observed upon the addition of $TBAHSO_4$ (10^{-3} in CH_3CN) and fitted to 1:2 (H:G) binding model of BindFit v0.5.

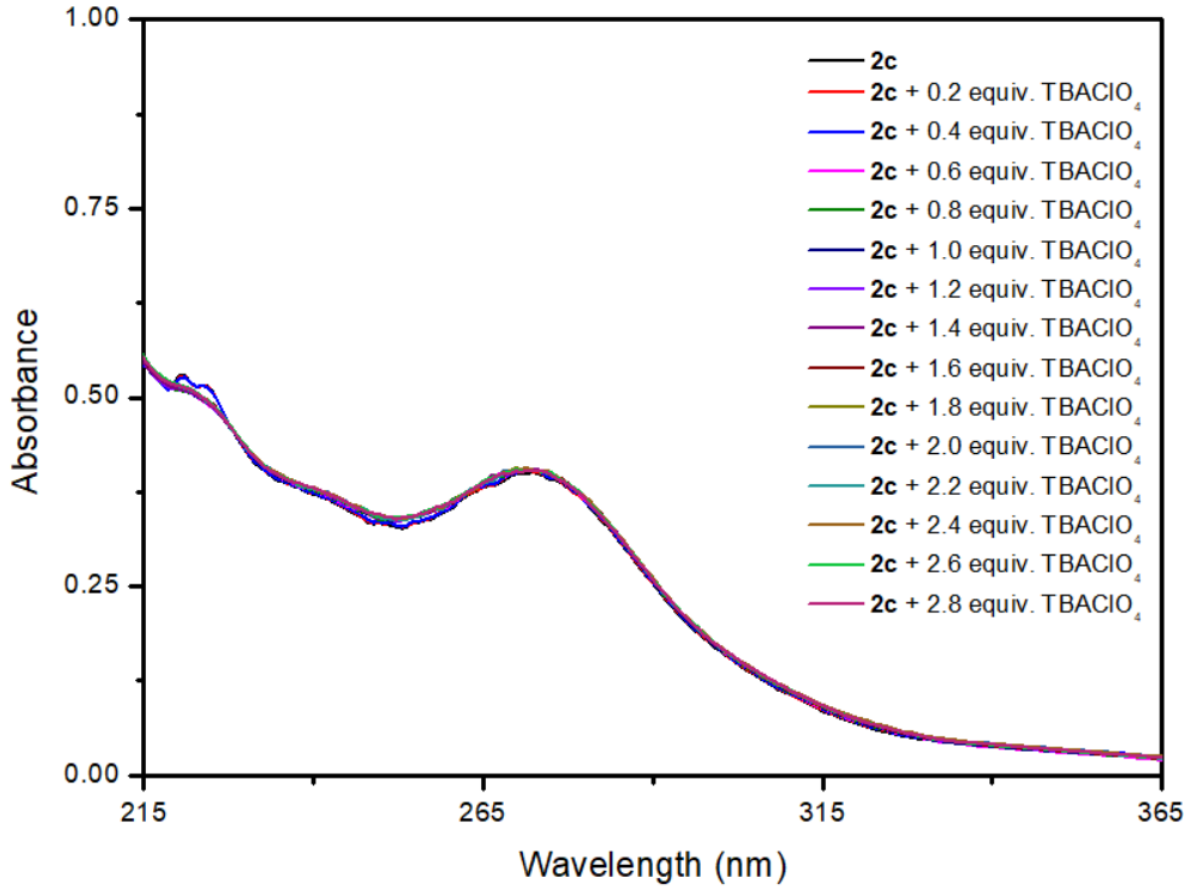

Figure S44: UV-vis spectrum of receptor **2c** (10^{-5} M in CH_3CN) observed upon the incremental addition of $TBACIO_4$ (10^{-3} M in CH_3CN).

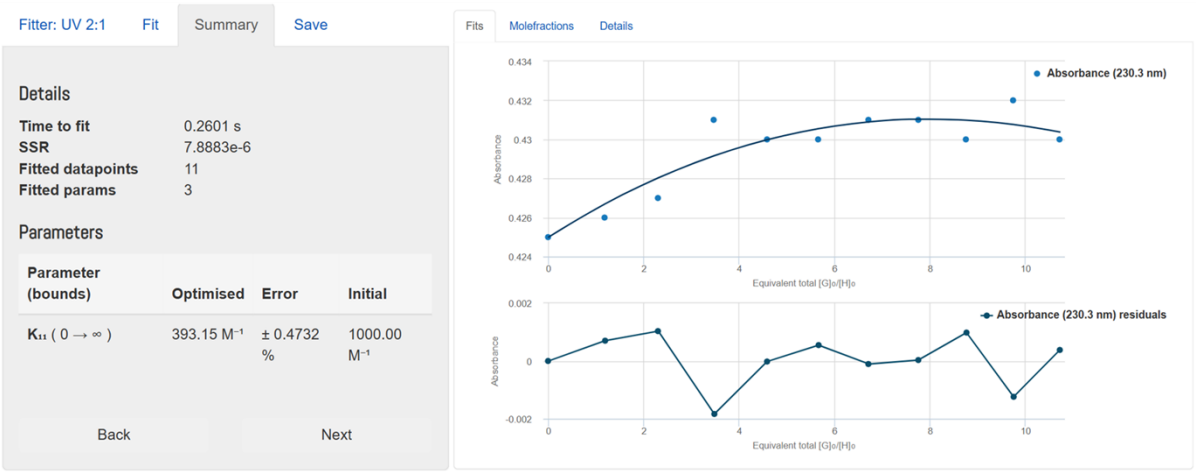

Figure S45: UV-vis absorbance titration data (at 230.3 nm) of receptor **2c** (10^{-5} M) observed upon the addition of TBAClO$_4$ (10^{-3} in CH_3CN) and fitted to 2:1 (H:G) binding model of BindFit v0.5.

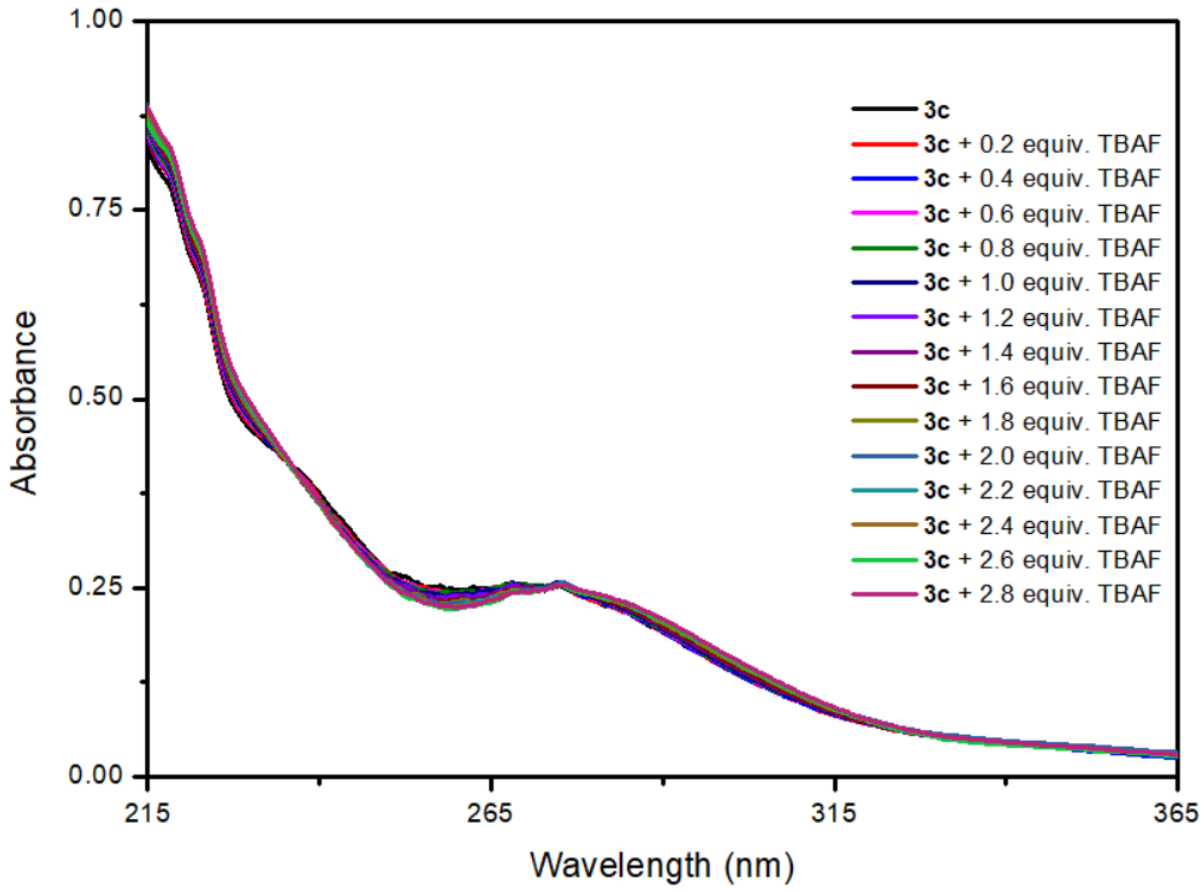

Figure S46: UV-vis spectrum of receptor **3c** (10^{-5} M in CH_3CN) observed upon the incremental addition of TBAF (10^{-3} M in CH_3CN).

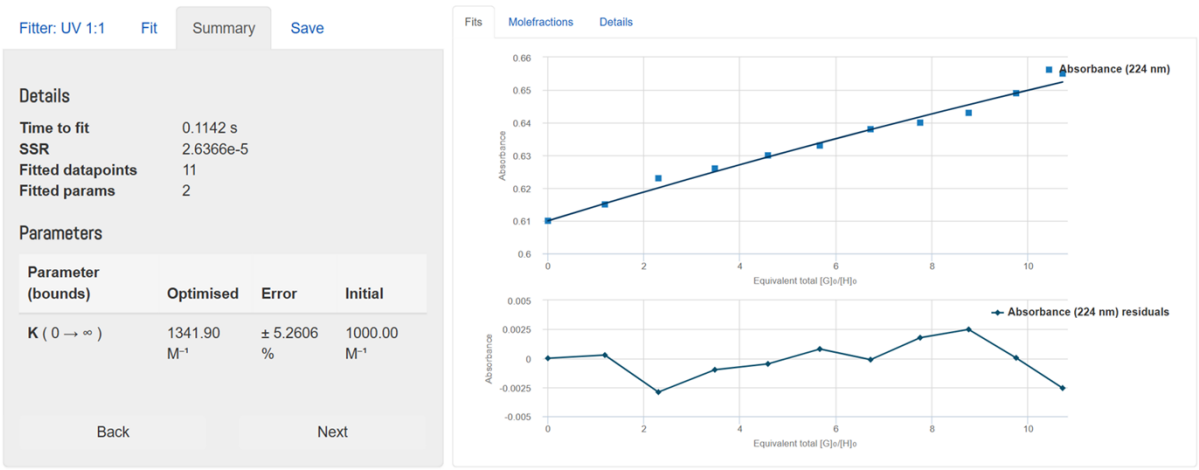

Figure S47: UV-vis absorbance titration data (at 224 nm) of receptor **3c** (10^{-5} M) observed upon the addition of TBAF (10^{-3} in CH_3CN) and fitted to 1:1 (H:G) binding model of BindFit v0.5.

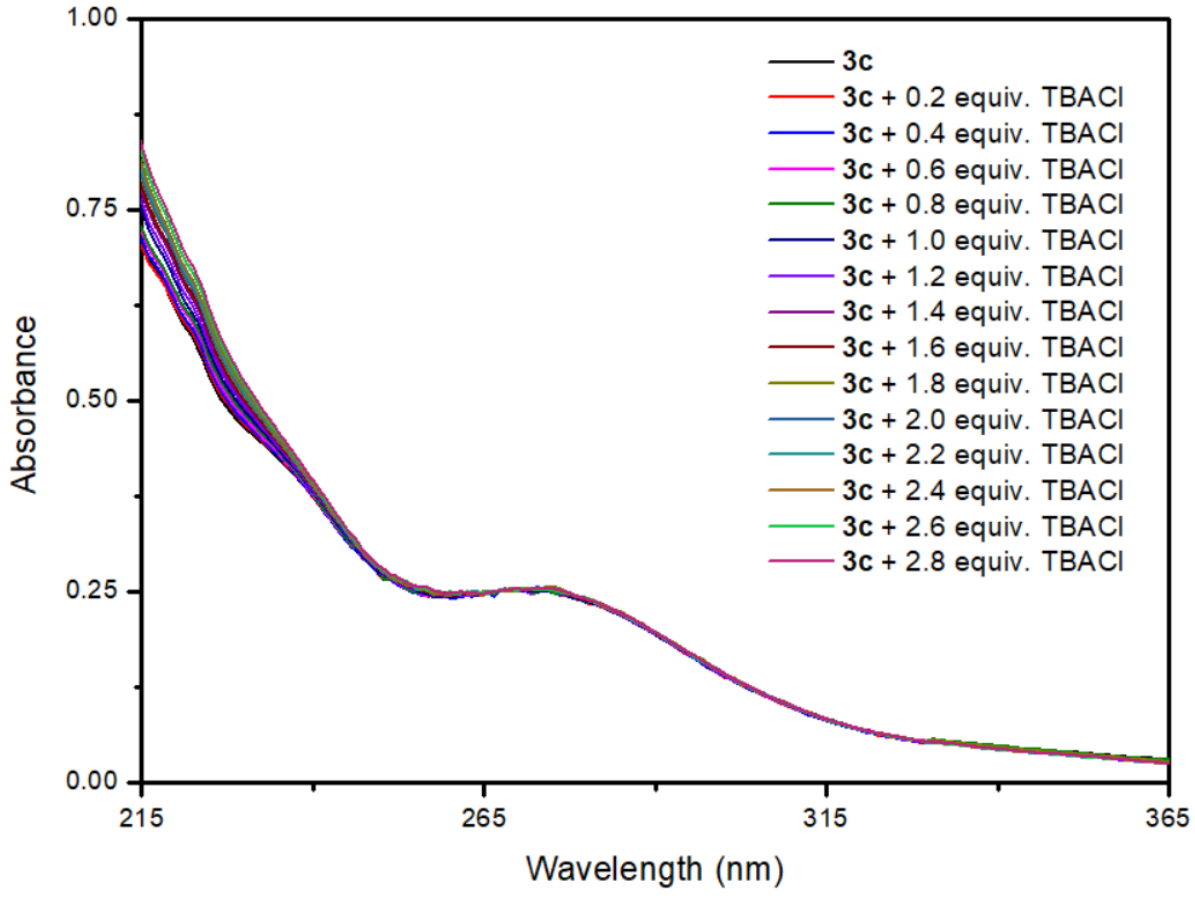

Figure S48: UV-vis spectrum of receptor **3c** (10^{-5} M in CH_3CN) observed upon the incremental addition of TBACl (10^{-3} M in CH_3CN).

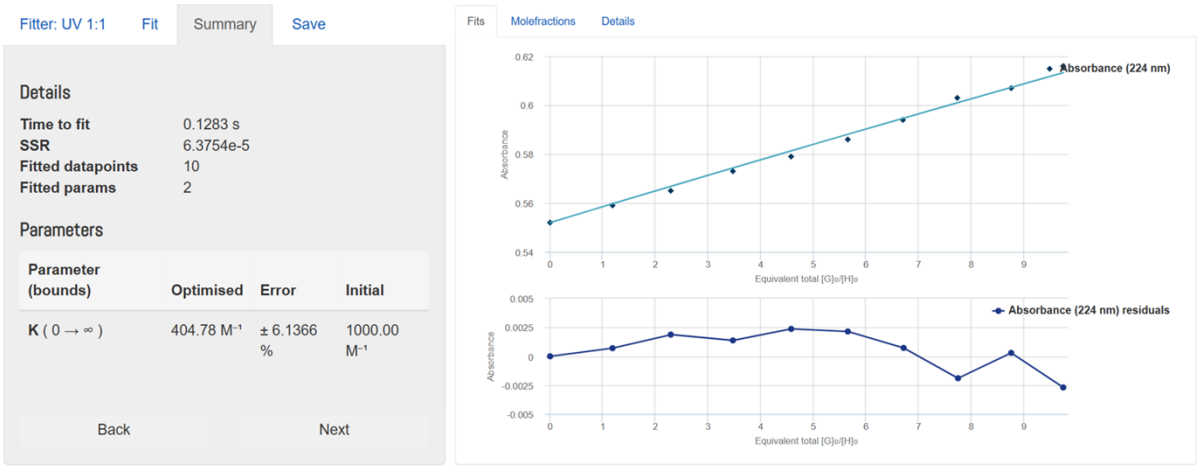

Figure S49: UV-vis absorbance titration data (at 224 nm) of receptor **3c** (10^{-5} M) observed upon the addition of TBACl (10^{-3} in CH_3CN) and fitted to 1:1 (H:G) binding model of BindFit v0.5.

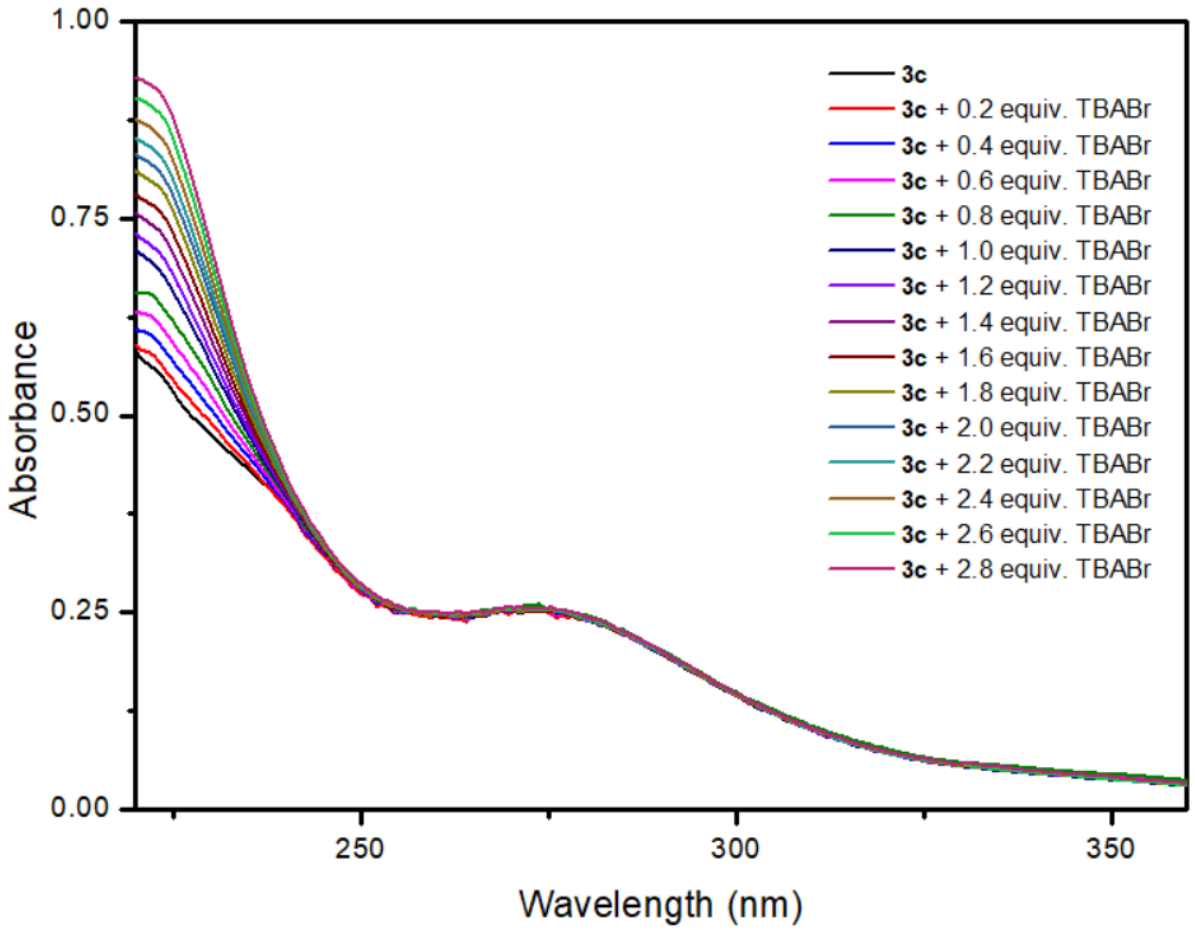

Figure S50: UV-vis spectrum of receptor **3c** (10^{-5} M in CH_3CN) observed upon the incremental addition of TBABr (10^{-3} M in CH_3CN).

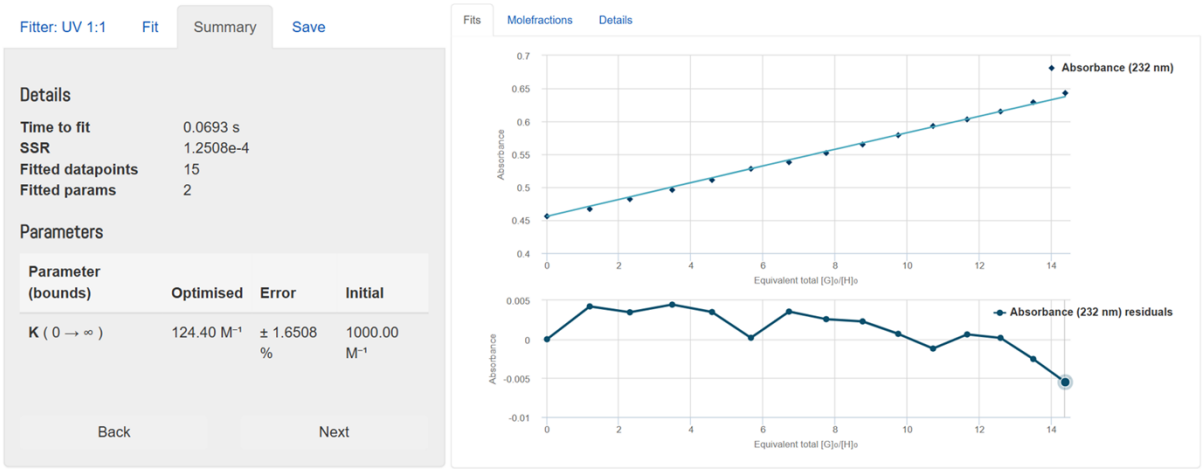

Figure S51: UV-vis absorbance titration data (at 232 nm) of receptor **3c** (10^{-5} M) observed upon the addition of TBABr (10^{-3} in CH_3CN) and fitted to 1:1 (H:G) binding model of BindFit v0.5.

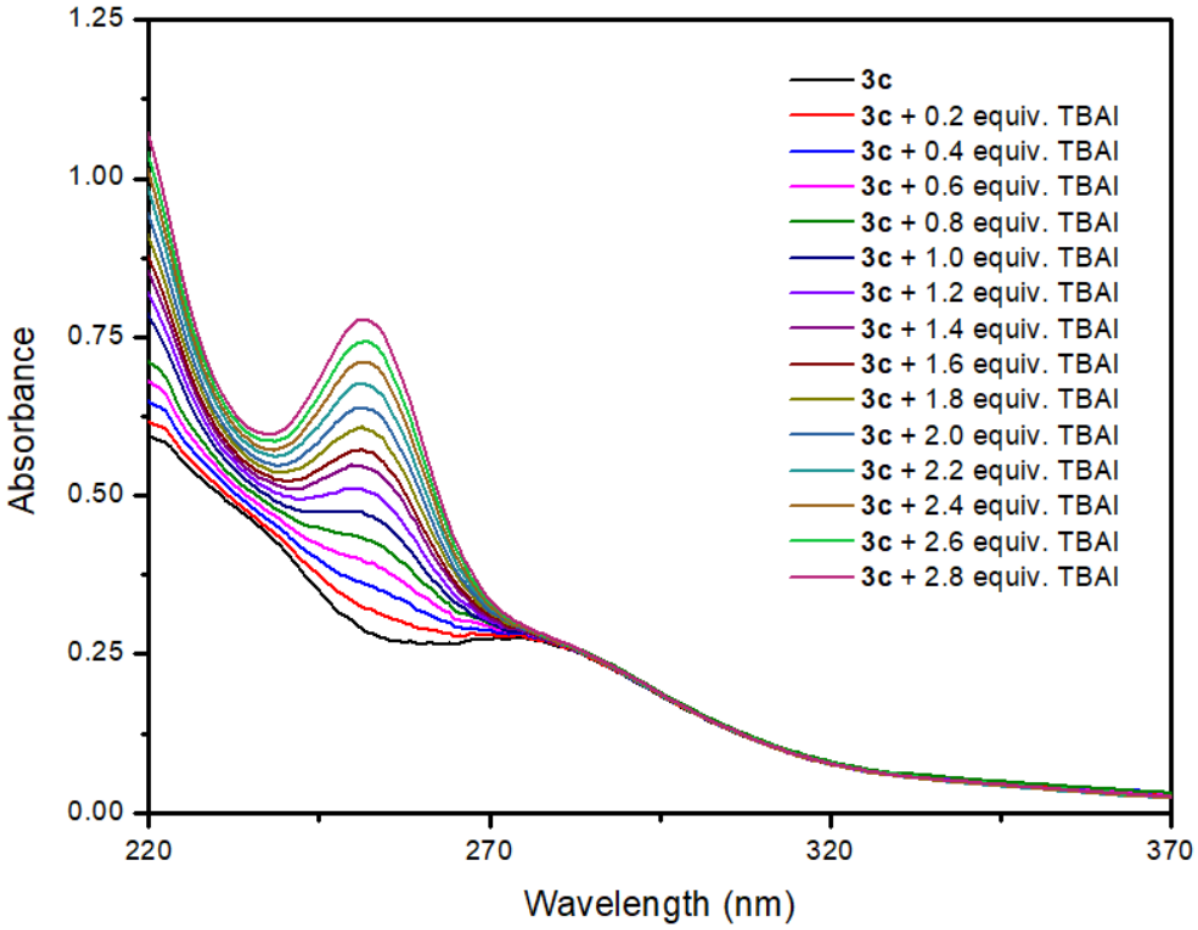

Figure S52: UV-vis spectrum of receptor **3c** (10^{-5} M in CH_3CN) observed upon the incremental addition of TBAI (10^{-3} M in CH_3CN).

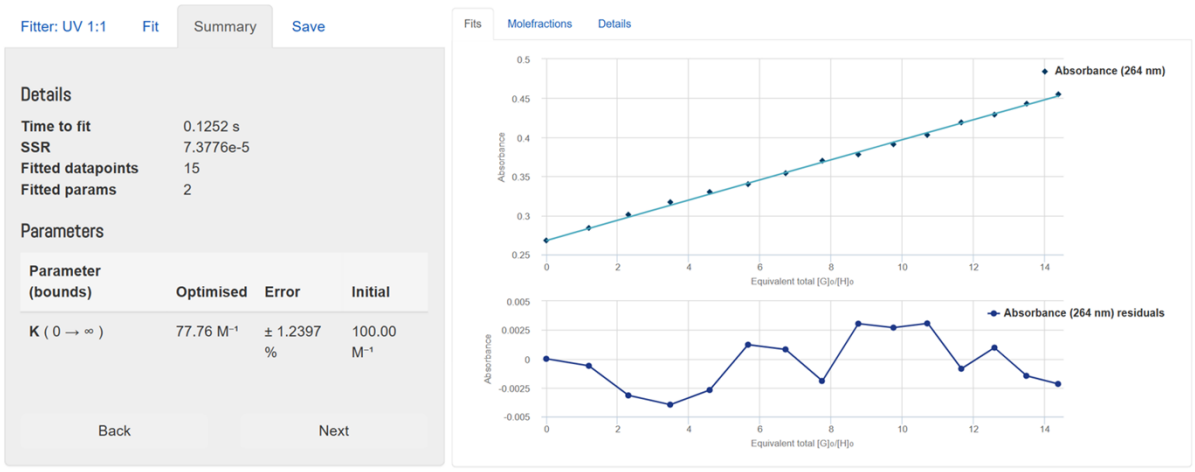

Figure S53: UV-vis absorbance titration data (at 264 nm) of receptor **3c** (10^{-5} M) observed upon the addition of TBAI (10^{-3} in CH_3CN) and fitted to 1:1 (H:G) binding model of BindFit v0.5.

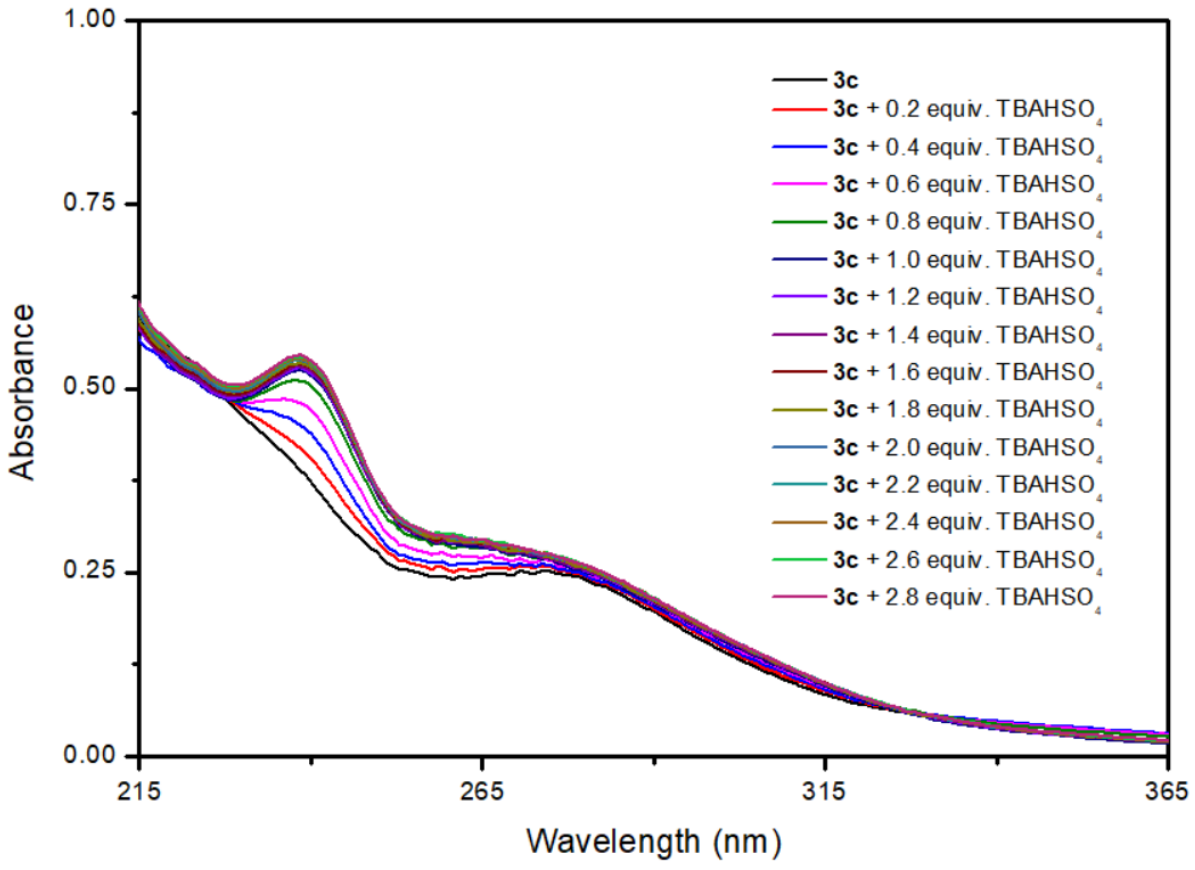

Figure S54: UV-vis spectrum of receptor **3c** (10^{-5} M in CH_3CN) observed upon the incremental addition of $TBAHSO_4$ (10^{-3} M in CH_3CN).

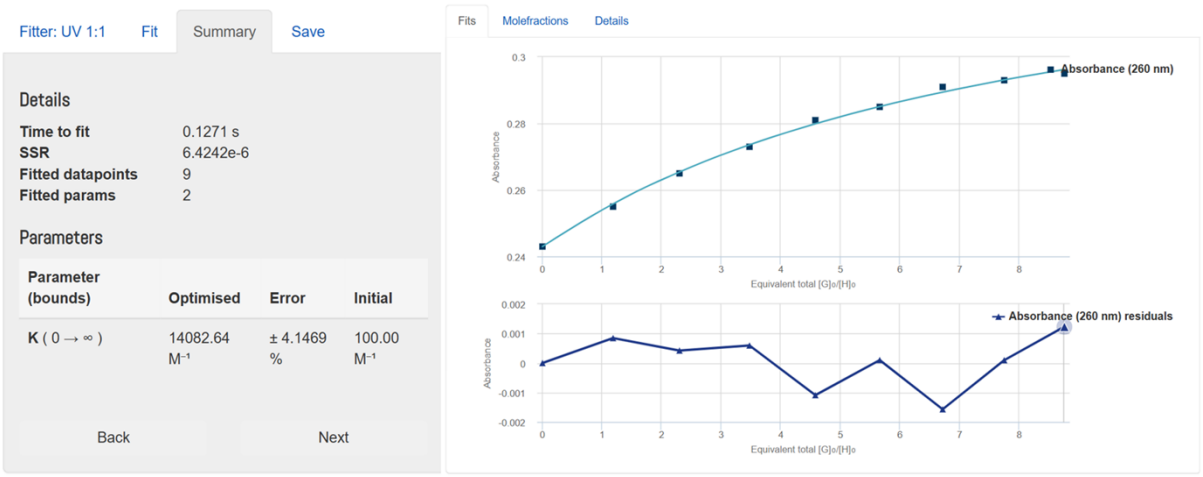

Figure S55: UV-vis absorbance titration data (at 260 nm) of receptor **3c** (10^{-5} M) observed upon the addition of $TBAHSO_4$ (10^{-3} in CH_3CN) and fitted to 1:1 (H:G) binding model of BindFit v0.5.

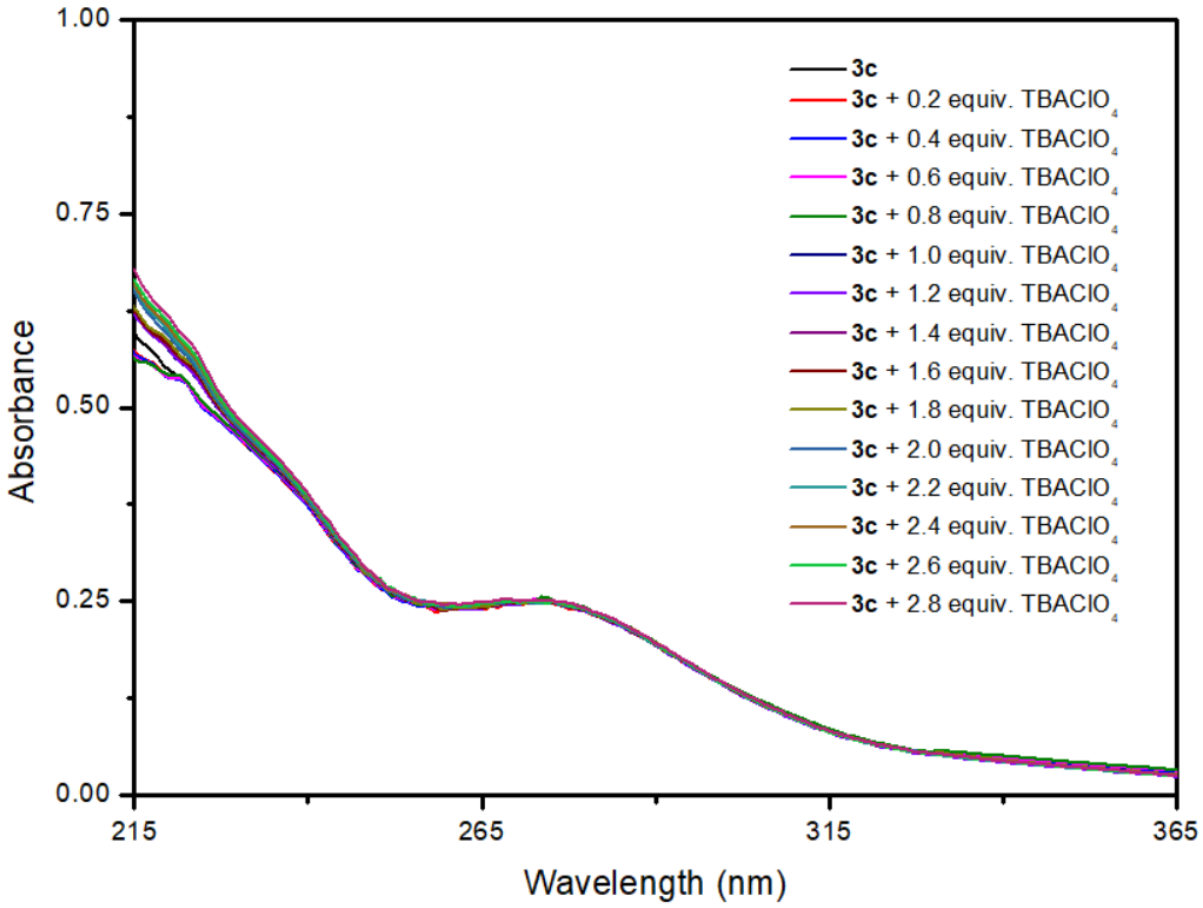

Figure S56: UV-vis spectrum of receptor **3c** (10^{-5} M in CH_3CN) observed upon the incremental addition of $TBACIO_4$ (10^{-3} M in CH_3CN).

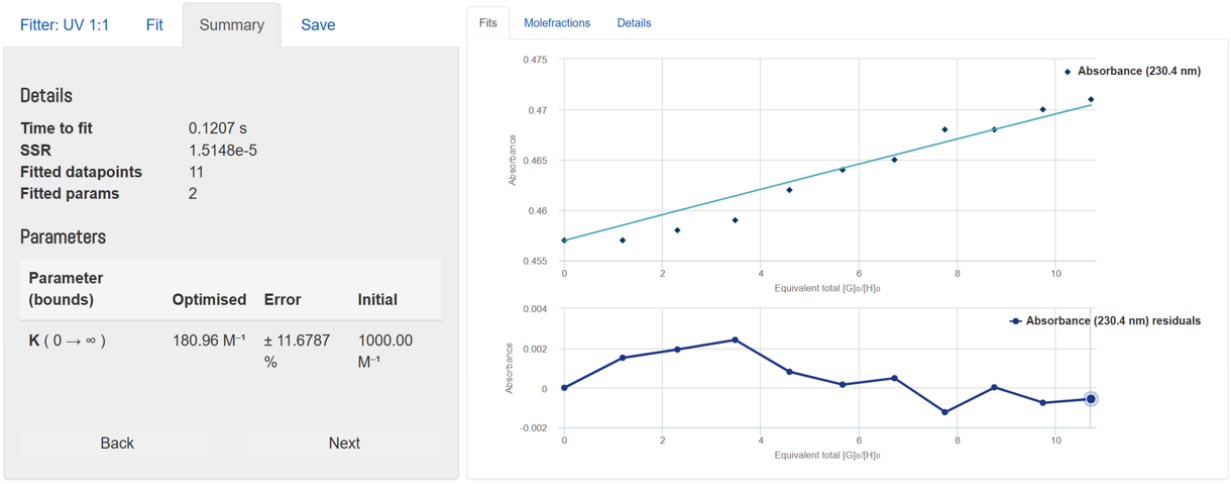

Figure S57: UV-vis absorbance titration data (at 230.4 nm) of receptor **3c** (10^{-5} M) observed upon the addition of $TBAClO_4$ (10^{-3} in CH_3CN) and fitted to 1:1 (H:G) binding model of BindFit v0.5.

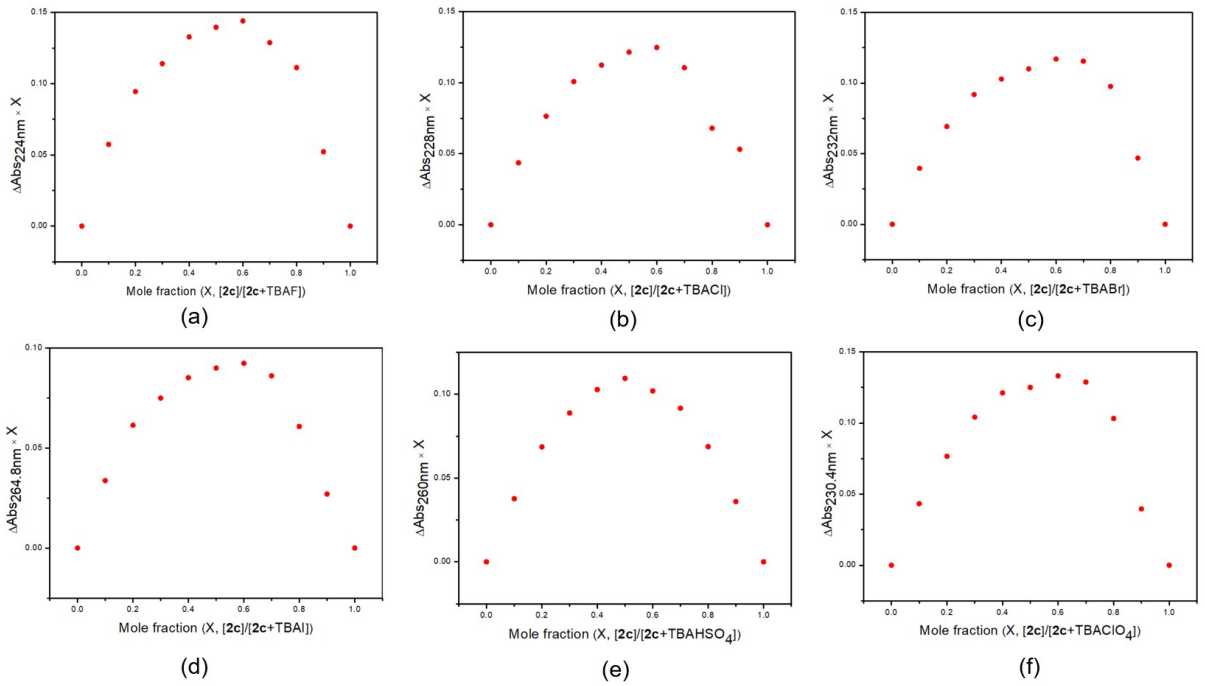

Figure S58: The Job's plots for **2c** with (a) TBAF (at 224 nm), (b) TBACl (at 228 nm), (c) TBABr (at 232 nm), (d) TBAI (at 264.8 nm) (e) $TBAHSO_4$ (at 260 nm), and (f) $TBAClO_4$ (at 230.4 nm) in CH_3CN. ([Host] = [Guest] = 10^{-5} M).

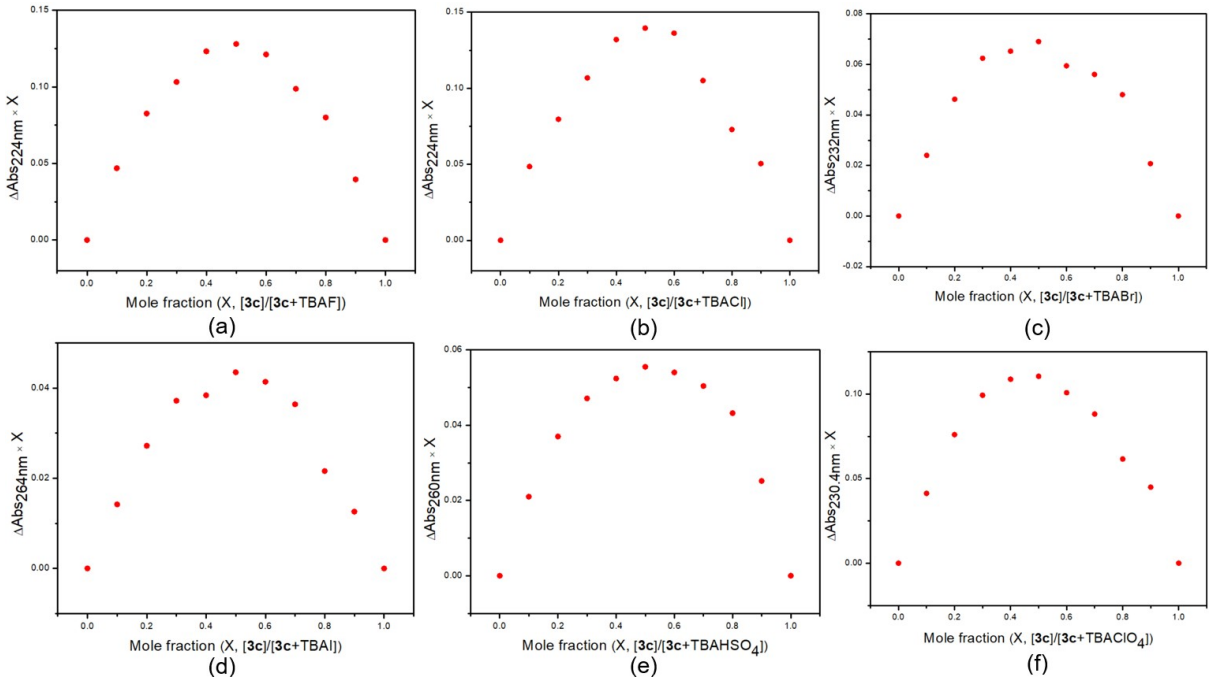

Figure S59: The Job's plots for **3c** with (a) TBAF (at 224 nm), (b) TBACl (at 224 nm), (c) TBABr (at 232 nm), (d) TBAI (at 264 nm), (e) $TBAHSO_4$ (at 260 nm) and (f) $TBAClO_4$ (at 230.4 nm) in CH_3CN. ([Host] = [Guest] = 10^{-5} M).

DFT studies:

Table S1: Relative energies (ΔE) of different conformations of azamacrocycles containing various *meso*-substituents.

Conformations	**3a**	**3b**	**3c**
	ΔE (kcal/mol)[a]		
1,3-*alternate*	0.00	+148.20	+150.70
1,2-*alternate*	+339.53	+170.91	+158.48
Cone	+173.66	0.00	0.00
Partial cone	+237.15	+69.50	+67.25

[a] relative to the most stable conformation.

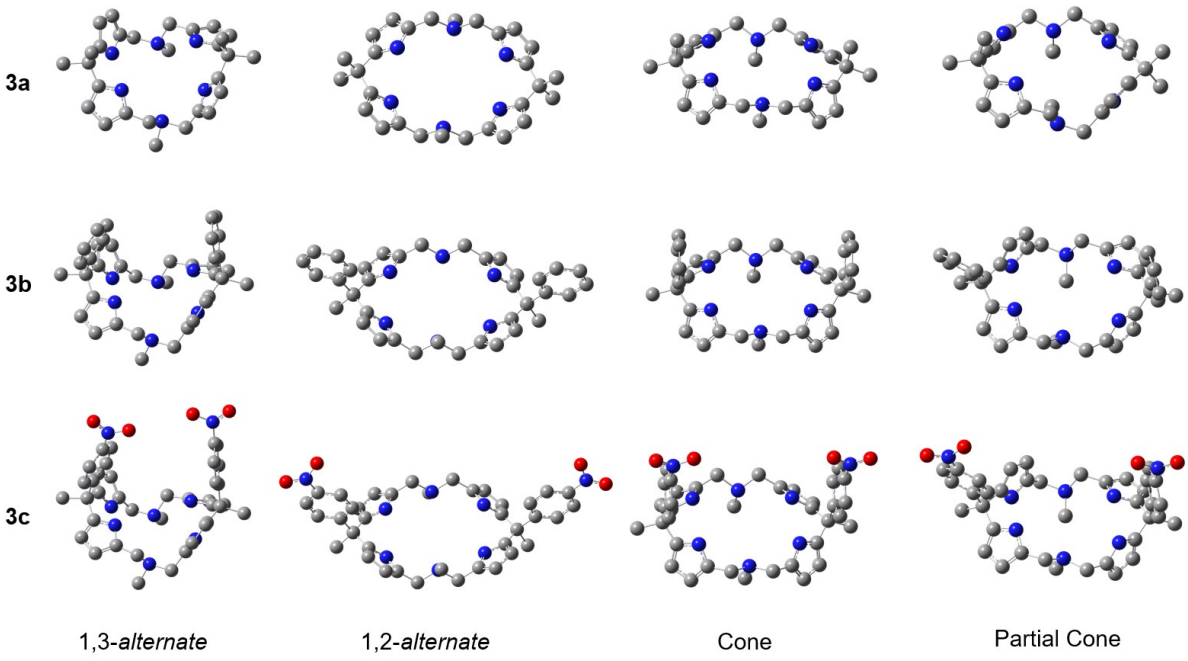

Figure S60: Four typical conformations of azamacrocyclic Mannich-bases (**3a-c**), optimized at the B3LYP/6-31G level in gas phase.

References

1. (a) A. J. F. N. Sobral, N. G. C. J. Rebanda, M. da Silva, S. H. Lampreia, M. R. Silva, A. M. Beja, J. A. Paixao and A. M. d'A. R. Gonzalves, *Tetrahedron Lett.*, 2003, **44**, 3971; (b) B. J. Littler, M. A. Miller, C. -H. Hung, R. W. Wagner, D. F. O'Shea, P. D. Boyle and J. S. Lindsey, *J. Org. Chem.*, 1999, **64**, 1391.

2. C. F. Macrae, I. Sovago, S. J. Cottrell, P. T. A. Galek, P. McCabe, E. Pidcock, M. Platings, G. P. Shields, J. S. Stevens, M. Towler and P. A. Wood, *J. Appl. Cryst.*, 2020, **53**, 226.

3. (a) M. J. Frisch, G. W. Trucks, H. B. Schlegel, G. E. Scuseria, M. A. Robb, J. R. Cheeseman, G. Scalmani, V. Barone, G. A. Petersson, H. Nakatsuji, X. Li, M. Caricato, A. V. Marenich, J. Bloino, B. G. Janesko, R. Gomperts, B. Mennucci, H. P. Hratchian, J. V. Ortiz, A. F. Izmaylov, J. L. Sonnenberg, D. Williams-Young, F. Ding, F. Lipparini, F. Egidi, J. Goings, B. Peng, A. Petrone, T. Henderson, D. Ranasinghe, V. G. Zakrzewski, J. Gao, N. Rega, G. Zheng, W. Liang, M. Hada, M. Ehara, K. Toyota, R. Fukuda, J. Hasegawa, M. Ishida, T. Nakajima, Y. Honda, O. Kitao, H. Nakai, T. Vreven, K. Throssell, J. A. Montgomery Jr., J. E. Peralta, F. Ogliaro, M. J. Bearpark, J. J. Heyd, E. N. Brothers, K. N. Kudin, V. N. Staroverov, T. A. Keith, R. Kobayashi, J. Normand, K. Raghavachari, A. P. Rendell, J. C. Burant, S. S. Iyengar, J. Tomasi, M. Cossi, J. M. Millam, M. Klene, C. Adamo,

R. Cammi, J. W. Ochterski, R. L. Martin, K. Morokuma, O. Farkas, J. B. Foresman and D. J. Fox, Gaussian 16, Revision C.01, Gaussian, Inc., Wallingford CT, 2016; (b) A. D. Becke, *J. Chem. Phys.*, 1993, **98**, 5648; (c) W. J. Hehre, R. Ditchfield and J. A. Pople, *J. Chem. Phys.*, 1972, **56**, 2257.